HHS Public Access

Author manuscript

Nat Commun. Author manuscript; available in PMC 2015 February 21.

Published in final edited form as:

Nat Commun. ; 5: 4664. doi:10.1038/ncomms5664.

Cardiac arrhythmia induced by genetic silencing of "funny" (f) channels is rescued by *GIRK4* inactivation

Pietro Mesirca[1,2,3], **Jacqueline Alig**[4], **Angelo G. Torrente**[1,2,3], **Jana Christina Müller**[5], **Laurine Marger**[1,2,3], **Anne Rollin**[1,2,3], **Claire Marquilly**[1,2,3], **Anne Vincent**[1,2,3], **Stefan Dubel**[1,2,3], **Isabelle Bidaud**[1,2,3], **Anne Fernandez**[5,6], **Anika Seniuk**[5,11], **Birgit Engeland**[4,7], **Jasmin Singh**[8], **Lucile Miquerol**[9], **Heimo Ehmke**[5,11], **Thomas Eschenhagen**[8,11], **Joel Nargeot**[1,2,3], **Kevin Wickman**[10], **Dirk Isbrandt**[4,7,*], and **Matteo E. Mangoni**[1,2,3,*]

[1]Département de Physiologie, Institut de Génomique Fonctionnelle, LabEx ICST, F-34094 Montpellier France

[2]UMR-5203, Centre national de la recherche scientifique, Universités de Montpellier 1 & 2, F-34094 Montpellier, France

[3]INSERM U661, Universités de Montpellier 1 & 2, F-34094 Montpellier, France

[4]Experimental Neuropediatrics, University Medical Center Hamburg-Eppendorf, 20246 Hamburg, Germany

[5]Department of Cellular and Integrative Physiology, Center for Experimental Medicine, University Medical Center Hamburg-Eppendorf, 20246 Hamburg, Germany

[6]Centre national de la recherche scientifique, UPR-1142, Institut de Génétique Humaine, F-34094, Montpellier, France

[7]Experimental Neurophysiology, University Hospital Cologne, 50937 Cologne, Germany, and German Center for Neurodegenerative Diseases (DZNE), 53175 Bonn, Germany

[8]Department of Experimental Pharmacology and Toxicology, Center for Experimental Medicine, University Medical Center Hamburg-Eppendorf, 20246 Hamburg, Germany

[9]Université Aix-Marseille, CNRS UMR 7288, Developmental Biology Institute of Marseille, Marseille, France

[10]Department of Pharmacology, University of Minnesota, Minneapolis, Minnesota 55455, USA

Correspondence: **Matteo E. Mangoni, PhD**, Institut de Genomique Fonctionnelle, Cardioprotection team-LabEx ICST, Departement de Physiologie, CNRS UMR 5203, Inserm U 661, University of Montpellier 1 and 2, 141, rue de la cardonille, 34094 Montpellier, France, matteo.mangoni@igf.cnrs.frwww.igf.cnrs.fr/recherche/axes-thematiques/physiology.

*Dirk Isbrandt and Matteo E. Mangoni are joint senior authors

Author contributions. P.M., J.A., H.E., K.W., J.N., B.E., D.I, T.E., and M.E.M designed research and edited the manuscript. P.M., J.A., A.G.T., L.M, A.S., B.E., A.R., A.V., C.M, S.D., I.B., A.F., J.S., T.E., and H.E. performed research and analyzed the results. P.M, D.I, and M.E.M wrote the paper.

Competing financial interests: The authors declare no competing financial interests.

[11]Cardiovascular Research Center Hamburg (CVRC) and DZHK (German Center for Cardiovascular Research), partner site Hamburg/Kiel/Luebeck, University Medical Center Hamburg-Eppendorf, Martinistraße 52, 20246 Hamburg, Germany

Abstract

The mechanisms underlying cardiac automaticity are still incompletely understood and controversial. Here we report the complete conditional and time-controlled silencing of the "funny" current (I_f) by expression of a dominant-negative, non-conductive HCN4-channel subunit (hHCN4-AYA). Heart-specific I_f silencing caused altered $[Ca^{2+}]_i$ release and Ca^{2+} handling in the sinoatrial node, impaired pacemaker activity, and symptoms reminiscent of severe human disease of pacemaking. The effects of I_f silencing critically depended on the activity of the autonomic nervous system. We were able to rescue the failure of impulse generation and conduction by additional genetic deletion of cardiac muscarinic G-protein-activated (GIRK4) channels in I_f-deficient mice without impairing heartbeat regulation. Our study establishes the role of f-channels in cardiac automaticity and indicates that arrhythmia related to *HCN* loss-of-function may be managed by pharmacological or genetic inhibition of GIRK4 channels, thus offering a new therapeutic strategy for the treatment of heart rhythm diseases.

Keywords

arrhythmia; electrophysiology; ion channels; sinoatrial node; pacemaker activity

Heart automaticity is a fundamental physiological function in animals. Pacemaker activity is generated by specialized, spontaneously active myocytes localized to the sinoatrial node (SAN). The SAN with its fastest spontaneous beating rate generates the cardiac impulse and controls the heartbeat. In the case of SAN failure, other components of the conduction system such as the atrioventricular node (AVN) and the His-Purkinje fiber (PF) network can also generate viable pacemaking[1]. Dysfunction in SAN automaticity underlies congenital or acquired bradycardia and bradycardia-associated conditions. Furthermore, it contributes to debilitating symptoms such as syncope, atrial fibrillation, heart failure, and causes sudden death[2–5]. SAN disease and conduction block account for more than 450,000 electronic pacemaker implantations each year in Europe and North America[6]. Thus, there is a strong interest in elucidating the mechanisms underlying cardiac pacemaking and impulse conduction at both the fundamental and clinical levels, and in finding alternative treatment options.

The ability of SAN cells to generate the pacemaker action potential is due to the diastolic depolarization phase during which the membrane voltage, from the end of an action potential, slowly depolarizes to reach the firing threshold for the succeeding one. The slope of the diastolic depolarization continuously modulates the heart rate and is regulated in opposite directions by the sympathetic and parasympathetic branches of the autonomic nervous system. Different classes of membrane ion channels, as well as ryanodine receptors (RyRs) of the sarcoplasmic reticulum, are involved in the generation and regulation of the diastolic depolarization (see[1] for review), but their specific functional roles are still incompletely understood. Among cardiac ion channels, f- (HCN) channels, underlying the

hyperpolarization-activated I_f current, are thought to play a major role in the generation and autonomic regulation of the diastolic depolarization in the SAN and in the cardiac conduction system[7,8], but its functional role is still matter of controversy[9]. A family of four homologous HCN-channel subunit isoforms (HCN1–4) was identified in mammals[10–13]. HCN4 is the predominant f-channel isoform in the mouse SAN and in the conduction system[14]. HCN1 and HCN2 are also present in the conduction system at varying expression levels[14,15]. Recent studies have indicated that human HCN4-channel mutations underlie congenital alterations in SAN pacemaking in humans, with variable symptoms ranging from mild or moderate bradycardia[16–18] to chronotropic incompetence[19], or atrioventricular conduction block with ventricular tachycardia[20]. *HCN4* knockout mice show a reduction of about 70% in I_f current associated with varying degrees of dysfunction in heart automaticity, ranging from recurrent SAN pauses with no significant change in heart rate and autonomic responsiveness[21,22] to lethal ventricular bradycardia and heart block[23]. These discrepancies could be explained by the different strategies of gene targeting adopted and/or by the presence of the other HCN-channel isoforms that can compensate for the loss-of-function of HCN4 channels in both the SAN and cardiac conduction system. Furthermore, deletion of the HCN4 protein may lead to alterations in the function of channel-associated proteins.

We thus developed a conditional transgenic mouse model expressing non-conducting hHCN4 subunits to suppress I_f conductance, independent of the endogenously expressed HCN subunits, in order to study the importance of this current in the generation and conduction of the cardiac impulse. We show that complete silencing of I_f alters intracellular Ca^{2+} handling in pacemaker myocytes and thus causes a complex disorder of cardiac rhythm, including SAN failure, atrioventricular block, and ventricular arrhythmia, which could be prevented by genetic inactivation of G-protein-activated (GIRK4) channels. In summary, our study provides a new animal model of human pathologies of heart rate and rhythm and identifies a new potential target for the treatment of bradycardia.

Results

Generation of conditional hHCN4-AYA-expressing transgenic mice

To suppress I_f conductance in a cardiac-specific and time-controlled manner, we generated double-transgenic mutant (Mut) mice expressing hHCN4-AYA dominant-negative subunits and a tetracycline-sensitive transactivator (tTA;[24]) under the control of an alpha-myosin heavy chain (αMHC) promoter[25]. In the absence of doxycycline (DOX), tTA binds to its promoter and drives the expression of an hHCN4 pore mutant construct in which a hemagglutinin (HA) epitope tag was added to the N-terminus and the selectivity filter motif was mutated to hHCN4-G480A/G482A (hHCN4-AYA; Fig. 1a). Two-electrode voltage-clamp recordings in Xenopus oocytes after coexpression of hHCN4-AYA cRNA with wild-type mHCN4 or mHCN2 cRNAs showed that mutated hHCN4-AYA protein affected mHCN2 and mHCN4 subunit-mediated currents in a dominant-negative manner (Supplementary Fig. 1a).

Heart-specific expression of hHCN4-AYA during pregnancy resulted in embryonic lethality, which is similar to what was described in homozygous $HCN4^{-/-}$ mice[26], because no double-transgenic mutant mice were born (+/T +/T, Fig. 1b. The likelihood of the other possible

genotypes was about 30% (n (+/+ +/+) = 33, n (+/+ +/T) = 24, n (+/T +/+) = 27). When hHCN4-AYA expression was suppressed by administering DOX to the mothers during pregnancy, the animals were born at a normal Mendelian ratio (n (+/+ +/+) = 62, n (+/+ +/T) = 52, n (+/T +/+) = 52, n (+/T +/T) = 54). DOX withdrawal at weaning induced expression of hHCN4-AYA, which was detectable after one week (Fig. 1c, Supplementary Fig. 1b). The expression level increased and resulted in a stronger protein signal after two to three weeks, reaching a maximum level after four weeks. The mutant hHCN4-AYA protein was detected in all cardiac chambers, with the highest expression in the atria (Fig. 1d, Supplementary Fig. 1b). To verify that the αMHC promoter effectively induced expression of hHCN4-AYA protein in pacemaker myocytes, we studied anti-HCN4 and anti-HA immunoreactivities by macro-confocal microscopy in preparations of the whole supraventricular stage of the heart containing the SAN and AVN of control (Supplementary Fig. 2) and mutant mice (Supplementary Fig. 3). Individual cells in the intact mutant SAN showed strong membrane-bound anti-HA immunoreactivity consistent with hHCN4-AYA protein expression (Fig. 1e). SAN-AVN preparations of the mutant heart displayed expression of hHCN4-AYA protein in all identifiable myocytes of the two heart pacemaker centers (Fig. 2). Inside the SAN region, the density of hCN4-AYA-expressing cells was particularly high in the site of origin of the pacemaker activity described in previous studies[27,28]. Like in SAN, hHCN4-AYA expressing cells were densely distributed throughout the whole AVN region (Fig. 2, Supplementary Fig. 3). No anti-HA immunoreactivity was found in preparations obtained from control mice (Supplementary Fig. 4). A significant population of hHCN4-AYA-expressing cells in the SAN and AVN stained positively against anti-HCN1 immunoreactivity (Fig. 2), which was also expressed in pacemaker cells of the SAN and AVN[14]. In addition, we performed immunostaining of enzymatically isolated SAN and AVN myocytes of control and mutant mice[29]. All myocytes isolated from mutant mice showed strong plasma membrane anti-HA immunoreactivity (Supplementary Fig. 5).

Expression of hHCN4-AYA in mutant mice silenced I_f conductance in SAN and conduction system

To evaluate the functional effects of hHCN4-AYA expression on I_f in the SAN and in the cardiac conduction system, we recorded I_f in control and mutant mice deprived of DOX after weaning. To unambiguously quantify current densities, we defined I_f as the net Ba^{2+}-insensitive and Cs^+-sensitive current[29,30] (Fig. 3). To record I_f in PF myocytes, we crossed control and mutant mice with *Cx40*$^{+/EGFP}$ mice (Mut/*Cx40* $^{+/EGFP}$, see Methods)[31]. In Mut/*Cx40*$^{+/EGFP}$ mice, PF myocytes were identified by EGFP epifluorescence. In comparison to controls, the averaged cellular capacitance was increased in mutant myocytes, indicating an increase in cell size in the conduction system of mutant mice (Supplementary Fig. 6). In myocytes isolated from control mice, the density of I_f was highest in SAN and lower in AVN and PF myocytes, as reported previously[32]. Unlike in control myocytes, I_f was drastically reduced at all membrane voltages tested in SAN, AVN, and PF myocytes isolated from mutant mice. We did not detect I_f at voltages spanning the diastolic depolarization range in all mutant myocytes tested (−75/−35 mV, Fig. 3).

I_f silencing slowed basal pacemaker activity and induced delayed afterdepolarization in SAN, AVN, and PF myocytes

Mutant SAN myocytes had significantly lower spontaneous firing rates than control myocytes and showed a strong reduction in the diastolic depolarization slope, both during the linear and exponential phases, as well as in the upstroke velocity (Supplementary Table 1). β-adrenergic receptor stimulation with submaximal (2 nM) or maximal (100 nM) concentrations of isoproterenol (ISO) increased the spontaneous beating rate in both control and mutant cells in a concentration-dependent manner. The difference in rate between mutant and control myocytes was present at all ISO concentrations tested (Fig 4a and b). Analysis of the action potential properties of mutant SAN myocytes under basal non-stimulated conditions revealed a more negative action potential threshold, prolonged action potential duration, and reduced action potential amplitude. Control and mutant SAN myocytes showed spontaneous diastolic depolarizations of the membrane potential (delayed afterdepolarizations, DADs) that did not elicit an action potential (Fig. 4a and c). Under basal conditions (no ISO), the frequency of DADs was significantly higher in mutant than in control myocytes (Fig. 4c). ISO significantly reduced the frequency of DADs in control but not in mutant myocytes (Fig. 4c). As a consequence, the frequency of DADs in mutant cells under ISO was more than tenfold higher than that recorded in control myocytes. The diastolic interval between a DAD and the following action potential under ISO was significantly longer than the cycle length between the two consecutive action potentials preceding the DAD (Fig. 4d), suggesting that DADs delayed the formation of the following pacemaker impulse. Similar results were obtained in mutant AVN and PF myocytes under basal conditions or ISO (Fig 4e–l). DADs were consistently recorded also in AVN and PF myocytes and displayed properties similar to those seen in SAN cells. Apart from longer action potential durations in mutant AVN cells, no differences were found in action potential parameters between mutant and control AVN and PF myocytes at baseline (Supplementary Table 1). The very low basal pacemaker activity recorded in mutant PF myocytes was also increased by ISO application, but – similar to our findings in SAN and AVN – the difference in spontaneous beating rates between control and mutant cells remained (Fig 4e and f). Taken together, our data show that I_f is critical for setting the basal spontaneous beating rate in SAN, AVN, and PF myocytes, but is not required for the sympathetic regulation of pacemaking in these structures. In addition, I_f silencing favored the induction of DADs in spontaneously beating myocytes.

I_f silencing induced augmented SR Ca^{2+} load and an increased frequency of local Ca^{2+} release events in SAN myocytes

The high frequency of DAD occurrence in I_f–deficient mutant myocytes isolated from the three rhythmogenic centers suggested altered Ca^{2+} handling and release in these cells[33]. We therefore recorded in control and mutant SAN cells voltage-dependent Ca^{2+} currents using voltage-clamp experiments and intracellular Ca^{2+} release ($[Ca^{2+}]_i$) by line-scan imaging of Fluo-4 loaded myocytes (Fig. 5). Quantification of voltage-dependent Ca^{2+} currents revealed an increased density of $I_{Ca,L}$, while the density and activation of $I_{Ca,T}$ were unchanged (Supplementary Fig.7). Consistent with our current clamp recordings (Fig. 4), the frequency of spontaneous $[Ca^{2+}]_i$ transients was reduced in mutant SAN cells (Fig. 5a).

Under basal conditions, mutant cells showed a significantly higher frequency of local Ca^{2+} release events (LCRs, Fig. 5b) and increased amplitude of $[Ca^{2+}]_i$ transients (Fig. 5c), indicating augmented SR Ca^{2+} load in these myocytes. Perfusion with ISO (100 nM) reduced the frequency of LCRs, but increased the frequency and reduced the amplitude of $[Ca^{2+}]_i$ transients (Fig. 5d) in mutant SAN cells. We did not observe differences in the upstroke velocity, duration, or recovery time of spontaneous $[Ca^{2+}]_i$ transients (Supplementary Fig. 8). We then directly tested the status of the SR Ca^{2+} load in isolated control and mutant SAN myocytes under ISO by rapid caffeine (10 mM) application. Caffeine–evoked Ca^{2+} release was significantly higher in mutant than in control cells, but the decay of Ca^{2+} release was similar in myocytes from the two mouse strains (Fig. 5e). Since it is known that SR Ca^{2+} overload favors the formation of $[Ca^{2+}]_i$ waves leading to Na^+/Ca^{2+} exchanger (NCX) activation–mediated DADs in cardiomyocytes,[34] we quantified the frequency of $[Ca^{2+}]_i$ waves (Fig. 5f and g). Under basal conditions and ISO, the frequency of $[Ca^{2+}]_i$ waves in mutant SAN myocytes (Fig. 5h and i) was comparable to the frequency of DADs (Fig. 4c). Under ISO, the diastolic interval between a $[Ca^{2+}]_i$ wave and the following spontaneous $[Ca^{2+}]_i$ transient was significantly longer than the cycle length between the two consecutive spontaneous $[Ca^{2+}]_i$ transients preceding the $[Ca^{2+}]_i$ wave (Fig. 5k). This observation is consistent with the hypothesis that $[Ca^{2+}]_i$ waves induced DADs in mutant myocytes.

I_f silencing induced bradycardia, atrioventricular blocks, and ventricular tachycardia in mutant mice

To investigate the consequences of I_f silencing in rhythmogenic centers in *vivo*, we performed telemetric ECG recordings in freely moving control and mutant mice. Since western blot analysis of hHCN4-AYA protein indicated that the transgene expression reached a plateau after five weeks following DOX withdrawal (week 0), we continuously analyzed the time course of ECG alterations for eight weeks after induction of transgene expression following DOX withdrawal. Heart rate (HR) of mutant mice constantly decreased and reached a plateau phase in week 6 (Fig. 6a). We did not record differences in heart rate of control mice during the entire 6-week period (495 ± 45 at week 0 and 508 ± 49 beats min^{-1} at week 6, n=3 $p>0.05$). At the same time, we observed a strong increase in the frequency of atrioventricular blocks (AVBs) in mutant mice (Fig. 6b). The decrease in heart rate (Fig. 6a) and increase in the occurrence of conduction abnormalities (Fig. 6b and c) approximately paralleled the kinetics of hHCN4-AYA protein expression (Fig. 1c). To investigate the reversibility of the phenotype of mutant mice, we reintroduced DOX to the diet at the end of week 8 to repress transgene expression. After four weeks of DOX reintroduction, AVBs disappeared, and the heart rates of control and mutant mice were comparable (Supplementary Fig. 9a and b). Furthermore, voltage-clamp recordings of mutant SAN myocytes showed normalized cell capacitance and I_f density four to five weeks after renewed administration of DOX to the food (Supplementary Fig. 9c and d). These observations demonstrate that the effects of hHCN4-AYA protein expression on heart rate are completely apparent after five weeks following DOX withdrawal and can be reversed by suppression of mutant subunit expression, indicating a causal relationship.

ECG recordings of mutant mice deprived of DOX after weaning showed that I_f silencing induced multiple and severe alterations in heart rate and rhythm. SAN activity of mutant mice was characterized by a prolonged SAN rate (PP intervals) and the presence of SAN pauses. Ventricular (RR) beating rates of mutant mice were also considerably lower in comparison to control animals (Fig. 6d). We recorded strongly prolonged atrioventricular conduction (PR) intervals in mutant mice (Fig. 6d). Both Mobitz type I and II AVBs were observed in mutant mice, but the frequency of type II Mobitz AVBs was higher than that of type I AVBs (Fig. 6e). During a 24-h recording period, maximum and minimum heart rates were lower in mutant than in control mice, but the absolute difference between maximum and minimum heart rates did not differ, showing a preserved degree of heart rate regulation (Fig. 6f). Consistent with the prominent effect of hHCN4-AYA expression on PF myocyte rhythmicity and DAD occurrence (Fig. 4), mutant mice also showed prolonged QRS complexes and frequent episodes of ventricular tachycardia in comparison to control mice (see below). Ventricular repolarization (QT and QTc intervals) was not affected in mutant mice (Fig. 6d). Since chronic bradycardia often goes along with cardiac hypertrophy[35], we investigated whether long-term transgene expression and bradycardia led to changes in left ventricular size and function in mutant mice. In line with telemetric recordings, echocardiography showed slower heart rates in mutant mice, but normal left ventricular and atrial mass to body weight ratios (Supplementary Fig. 10). Left ventricular end-diastolic volume, stroke volume, and area shortening under control and stimulated conditions did not differ between control and mutant mice (Supplementary Fig. 10). Recordings showed a tendency toward a reduced cardiac output in mutant mice, but this difference did not reach statistical significance (Supplementary Fig. 10). Furthermore, mutant mice did not show alterations in blood pressure measured by means of radiotelemetry as a function of locomotor activity in the home cage (Supplementary Fig. 11).

Heart rate of mutant mice was insensitive to the I_f inhibitor ivabradine

To investigate whether I_f silencing in mutant mice corresponded to the elimination of the pharmacological sensitivity of heart rate to I_f inhibition, we recorded ECGs of control and mutant mice upon injection of ivabradine, a selective I_f inhibitor[36]. Administration of ivabradine (6 mg/kg) reduced the heart rate in control, but not in mutant mice (Fig. 7a and b). No ivabradine effect was detected in mutant mice when considering the ventricular (RR interval, Fig. 7b) or SAN rates (PP interval, Fig. 7c). Remarkably, heart rates and SAN rates of ivabradine-treated control mice and untreated mutant mice were similar (Fig. 7d), indicating that the negative chronotropic effect of ivabradine was completely abolished. Likewise, ivabradine had no effect in isolated spontaneously beating right atrial preparations from mutant mice (Supplementary 12), but it caused a slowly developing, concentration-dependent decrease in spontaneous beating rates in control atria, which were comparable to those observed in mutant SAN myocytes perfused with ISO (Supplementary Fig. 12). In agreement with these results, ivabradine slowed pacemaker activity of isolated control SAN myocytes by about 33% but did not affect the spontaneous beating rate of mutant myocytes (Fig. 7e). These observations indicate that no residual, physiologically relevant I_f current was present in hCN4-AYA-expressing mutant SAN myocytes.

Autonomic nervous system activity modulated the functional impact of I_f silencing on heart rate and impulse conduction

We then investigated the impact of I_f silencing on *in vivo* heart rate regulation. Pharmacological inhibition of the sympathetic branch of the autonomic nervous system by propranolol (5 mg/kg) significantly decreased the heart rates of control mice, but had no effect on those of mutant mice (Fig. 8a). Propranolol reduced the heart rate of control mice to levels that did not differ from those of mutant mice, either under basal conditions or in the presence of propranolol (Fig. 8a). Likewise, combined injection of propranolol and atropine (0.5 mg/kg), an inhibitor of the parasympathetic input, did not significantly affect the heart rate of mutant mice (Fig. 8b). Interestingly, pharmacological inhibition of the autonomic input by combined injection of atropine and propranolol strongly reduced the number of AVBs in mutant mice (Fig. 8c and d). These observations indicate that the physiological impact of I_f silencing on heart rate determination and impulse conduction was reduced in the absence of autonomic input.

I_f silencing did not impair maximal β-adrenergic regulation of heart rate

We then assessed the capability of mutant mice to increase their heart rate under conditions of maximal sympathetic input, that is, direct pharmacological stimulation of β-adrenergic receptors or physical exercise. Injection of ISO or atropine similarly increased the heart rate in both control and mutant mice (Fig. 8e–g). Contrary to the inhibition of the autonomic nervous system (Fig. 8d), ISO did not reduce cardiac dysrhythmia due to SAN pauses and AVBs (Fig. 8e). Comparable results were obtained from ISO-stimulated, spontaneously beating right atria preparations (Supplementary Fig. 10c). Although the maximum heart rate in ISO-stimulated mutant mice did not reach that of control mice (Fig. 8f), the relative extent of ISO-induced increase did not differ between the two strains (Fig. 8h). Likewise, during a swimming test combining mental stress with physical activity (Fig. 8g and h), the heart rate was increased to an extent similar to that in control mice. Taken together, these data show that in spite of complete I_f silencing the autonomic nervous system was still capable of regulating heart rate.

Genetic inactivation of GIRK4 channels ameliorated SAN failure, atrioventricular dysfunction, and ventricular arrhythmia in mutant mice

Since the impact of I_f silencing on heart rate and atrioventricular dysfunction depended on the status of the autonomic nervous system, we investigated the possibility of counterbalancing I_f loss-of-function in mutant mice by reducing the influence of the parasympathetic nervous system on heart rate and atrioventricular conduction. We thus crossed mutant mice with *GIRK4* (*Kir3.4*) knockout mice (*GIRK4*$^{-/-}$) deficient in the cardiac G-protein-gated inwardly rectifying K^+ current I_{KACh}[37] to obtain double-mutant Mut/*GIRK4*$^{-/-}$ mice. Telemetric 24-hour ECG recordings in Mut/*GIRK4*$^{-/-}$ mice showed a higher heart rate in comparison to mutant animals, although the mean RR interval measured in double-mutant mice was still significantly longer than that of controls (Fig. 9a). The SAN rates (PP interval) of Mut/*GIRK4*$^{-/-}$, and of mutant mice did not differ from each other (Fig. 9b). However, SAN pauses were absent in Mut/*GIRK4*$^{-/-}$, mice, indicating that *GIRK4* loss-of-function improved SAN function. The PR interval was significantly shorter in Mut/

GIRK4$^{-/-}$ mice, although it was still longer than that in control mice (Fig 9c). The occurrence of AVBs was drastically reduced in Mut/*GIRK4*$^{-/-}$, suggesting that the activity of GIRK4 channels in the AVN contributed to conduction dysfunction in mutant mice (Fig. 9d). Loss of GIRK4 channels did not normalize QRS intervals, which were similarly prolonged in Mut/*GIRK4*$^{-/-}$ and mutant mice (Fig 9e). In most cases, the ventricular tachycardia/tachyarrhythmia observed in mutant mice was preceded by dysfunction of atrial rhythm or AVBs. In particular, SAN pauses and AVBs preceded ventricular tachycardia in more than 70% of cases, suggesting a causal relationship (Fig. 9j). In line with the absence of SAN pauses and AVBs in Mut/*GIRK4*$^{-/-}$ mice, we did not record ventricular tachycardia or extrasystoles in these animals (Fig. 9k, Table 1). Like control and mutant mice, Mut/*GIRK4*$^{-/-}$ animals showed a preserved degree of heart rate regulation and a normal recovery of resting heart rate following direct β-adrenergic stimulation (Supplementary Fig. 11). These data indicate that the inactivation of GIRK4 channels was effective in improving SAN automaticity and atrioventricular conduction and in preventing ventricular arrhythmias in I_f-deficient mice (Table 1).

Discussion

Cardiac pacemaker activity is a complex phenomenon requiring the interaction of different classes of membrane ion channels[1], $[Ca^{2+}]_I$ cycling[38], and probably other mechanisms yet to be identified. The "funny" current I_f is thought to play a key role in the generation and regulation of automaticity in the adult heart[8], but its functional role and importance are still incompletely understood[9,21]. Pharmacological[39] and genetic studies in humans[16–19] indicate a role for I_f in the determination of heart rate and rhythm. However, a body of data obtained from mouse models in which HCN4 subunits were deleted showed contrasting results in relation to the importance of these channels in SAN pacemaking and impulse conduction[21–23]. Furthermore, although several groups described the phenotype of mice deficient in HCN1[15], HCN2[40], or HCN4[21,23,41] subunits, no mouse model has yet been available that shows a suppression of I_f conductance of up to >95% of its control value. In this study, we show for the first time heart-specific and time-controlled silencing of I_f conductance in both the SAN and the conduction system. We show that chronic functional ablation of I_f conductance induces severe abnormalities of both atrial and ventricular rhythms by altering Ca^{2+} handling in pacemaker myocytes. The resulting complex cardiac arrhythmia could be prevented by inactivation of GIRK4 channels.

We used the Tet-off strategy to express mutant hHCN4-AYA non-conducting subunits to suppress f-channel conductance in a dominant-negative manner. Using this experimental approach, we achieved I_f silencing without deletion of HCN-channel subunits from the plasma membrane and thus without depletion of HCN-associated proteins. Embryonic lethality observed when mutant hHCN4-AYA channels are expressed during embryonic development suggests that I_f conductance is required for the embryonic heart to be viable (Fig.1), which is compatible with the phenotype of both global and heart-specific HCN4 knockout mice[26]. Western blot experiments demonstrated that the hHCN4-AYA protein was highly expressed in the atria and ventricles of adult mutant mice (Fig. 1). Similar to findings from immunostainings of native HCN4 channels of SAN and AVN preparations (Fig. 2), or of isolated myocytes, for hHCN4-AYA protein (Supplementary Fig. 5) indicated that the

mutant channel protein was targeted to the cell membrane. Consistent with the immunostaining in mutant pacemaker tissue and the dominant-negative effect on HCN4- and HCN2-mediated currents by hHCN4-AYA recorded in Xenopus oocytes, I_f was abolished at voltages spanning the diastolic depolarization range of myocytes from the SAN and the conduction system (Fig. 3). I_f silencing throughout the conduction system suggested that mutant hHCN4-AYA channels exerted a dominant-negative effect, also on native HCN1 channels. In agreement with the complete silencing of I_f, pacemaker activity of mutant SAN myocytes, intact atrial preparations, and the *in vivo* heart rate of hHCN4-AYA mutant mice were insensitive to ivabradine (Fig. 6, Supplementary 12). The reasons for the increase in cell membrane capacitance in mutant myocytes are unclear at present. Since mutant and Mut/*GIRK4*$^{-/-}$ SAN myocytes showed similar membrane capacitance (Supplementary Fig. 6), we can exclude that this phenomenon is due to cellular hypertrophy secondary to chronic AVBs. We thus speculate that the increase in cell size in mutant myocytes represents an adaptive mechanism to increased SR Ca^{2+} load (Fig. 5).

Action potential recordings of myocytes from the heart-rhythmogenic centers and Ca^{2+} imaging of mutant SAN myocytes showed that I_f silencing had strong effects on pacemaker activity and $[Ca^{2+}]_i$ handling in these cells. Mutant myocytes displayed slow diastolic depolarization (Fig. 4a, e and i) and a high incidence of DADs (Fig. 4c, g and k). hHCN4-AYA expression induced a 76% reduction in the basal spontaneous beating rate in SAN myocytes, 51% in AVN, and 67% in PF myocytes (Fig. 4). β-adrenergic activation by ISO abolished the differences in action potential amplitude and duration between control and mutant SAN and AVN myocytes (Supplementary Table 1). We attribute these differences to a partial loss of Ca^{2+} -activated SK channel activity[42] secondary to low cellular spontaneous beating rate, which induces low rate-dependent opening of $Ca_v1.3$ channels[43]. Perfusion of ISO stimulates $Ca_v1.3$ channels[44] and could also activate mERG1 channels, thereby normalizing action potential duration[45]. The increased SR Ca^{2+} load in mutant SAN myocytes induced spontaneous, partially synchronized openings of RYRs, thereby forming $[Ca^{2+}]_i$ waves[34] (Fig. 5). It is well established that SR Ca^{2+} overload–mediated $[Ca^{2+}]_i$ waves activate the NCX, thus depolarizing the membrane potential and causing DADs[46]. Consistent with this view, DADs in mutant SAN myocytes were generated by spontaneous $[Ca^{2+}]_i$ waves, presumably because of SR Ca^{2+} overload (Fig. 5e). Such a mechanism would also explain the increased frequency of spontaneous $[Ca^{2+}]_i$ sparks recorded in mutant myocytes (Fig. 5e).

Two non-mutually exclusive phenomena may account for SR Ca^{2+} overload in mutant SAN myocytes. First, mutant myocytes showed augmented density of peak $I_{Ca,L}$ (Supplementary Fig. 7) translating into increased Ca^{2+} entry during the action potential upstroke and Ca^{2+} uptake in the SR during the decaying phase of the $[Ca^{2+}]_i$ transient. Second, the slow diastolic phase of mutant myocytes can increase the SR Ca^{2+} load via longer SERCA–mediated Ca^{2+} uptake before an action potential eventually occurs. Although β-adrenergic activation by ISO increased pacemaker activity, the difference in spontaneous beating rate between control and mutant myocytes was still 61% in SAN, 43% in AVN, and 42% in PFs (Fig. 4). These observations are consistent with data on Ca^{2+} handling. Even though ISO appeared to facilitate RyR-dependent Ca^{2+} release, it only incompletely normalized spark

frequency and SR Ca^{2+} overload. Similarly, ISO did not reduce DADs or $[Ca^{2+}]_i$ waves in mutant myocytes (Fig.4 and 5). Although we did not directly investigate the mechanistic link between $[Ca^{2+}]_i$ waves and delayed formation of the following pacemaker action potential under ISO, previous work by other groups indicates that diminished SR Ca^{2+} load delays the formation of spontaneous $[Ca^{2+}]_i$ transients[47] and that Ca^{2+} uptake is directly linked to the rate of pacemaking in rabbit SAN myocytes[48]. It is possible that $[Ca^{2+}]_i$ waves drive the SR into a partially depleted state, thus preventing rapid generation of the following pacemaker impulse. Taken together, our data demonstrate that I_f silencing impairs pacemaker activity of automatic myocytes by eliminating f-channel activity in the diastolic depolarization, which leads to altered $[Ca^{2+}]_i$ release and Ca^{2+} handling.

Consistent with I_f silencing in the three main rhythmogenic centers of the heart, *in vivo* heart rate of mutant mice was reduced by 36%. Mutant mice displayed a significant reduction in SAN activity, which was reflected in frequent pauses and an 18% slowing of the SAN rate (Fig. 5), a value that matches that recorded in healthy human volunteers treated with the I_f blocker ivabradine[39]. In spite of significant SAN dysfunction, we did not find evidence of a reduction in the sympathetic regulation of heart rate in hHCN4-AYA mutant mice. Indeed, spontaneously beating myocytes (Fig. 4), intact atrial preparations (Supplementary Fig. 12), or *in vivo* heart rate (Fig. 5) showed a preserved degree of regulation. Likewise, the relative increase in heart rate after injection of atropine, ISO, or following stress did not differ between control and mutant mice, demonstrating that the compliance of the sympathetic regulation of heart rate was preserved under conditions of I_f silencing (Fig. 7). We attribute the preserved heart rate regulation in mutant mice to the capability of β-adrenergic activation to partially increase RYR-dependent Ca^{2+} release[49,50] in mutant SAN myocytes (Fig. 5), as well as to stimulation of other mechanisms involved in automaticity such as $I_{Ca,L}$[44] and CaMKII[51].

Although I_f silencing obviously did not impair maximum β-adrenergic regulation of pacemaking, our data show that the importance of I_f in the determination of *in vivo* heart rate and atrioventricular conduction was dependent on the activity of the autonomic nervous system. Indeed, pharmacological inhibition of the β-adrenergic tone by propranolol abolished the difference in basal heart rate between control and mutant mice (Fig. 8). Likewise, the “intrinsic” *in vivo* heart rate measured upon combined administration of atropine and propranolol did not significantly differ between control and mutant mice (Fig. 8b), which is consistent with our previous finding that inhibition of the autonomic nervous system input did not affect the heart rate of mice with conditional abolition of cAMP-dependent I_f regulation[52]. These observations suggest that in freely moving mice the establishment of resting heart rate *in vivo* by the autonomic nervous system involves I_f. In comparison, the setting of intrinsic heart rate under conditions of autonomic nervous system inhibition is less dependent on f-channel activity. The finding of similar intrinsic SAN rates measured *ex vivo* in isolated control and in mutant atrial preparations is in line with this concept (Supplementary Fig. 12). However, isolated atrial preparations are mechanically unloaded, while blood flow-induced mechanical forces cyclically challenge the SAN *in vivo*. Thus, it is possible that mechano-electric feedback in SAN myocytes or fibroblasts[53] contributes to pacemaking *in vivo*, especially under conditions of I_f silencing. The similar

spontaneous beating rate of control and mutant atria is likely to be due to the combined compensatory effects of the well-known phenomenon of “pacemaker shift” of the dominant pacemaker site within the SAN[54] to a region that is less sensitive to I_f silencing[55], and to the augmented $I_{Ca,L}$ density in mutant SAN myocytes (Supplementary Fig. 7). A shift of the leading pacemaker site *in vivo* may also explain, at least in part, the different effects of hHCN4-AYA expression on the pacemaker activity in SAN myocytes *in vitro* and on the SAN *in vivo* (PP interval). Joung et al. have reported that DADs that fail to trigger a local action potential prevent the subsequent SAN activation in intact SAN preparations[56]. We thus propose that $[Ca^{2+}]_i$ wave-induced DADs recorded in mutant SAN myocytes underlie SAN pauses recorded *in vivo*. Furthermore, the delay in the coupling time between a DAD and the following action potential is an additional mechanism explaining SAN pauses and bradycardia in mutant mice.

SAN bradycardia in mutant mice was always accompanied by strongly impaired atrioventricular conduction. The PR interval of conducted SAN impulses was almost double of that in control animals, and all mice investigated showed a high frequency in second-degree atrioventricular blocks (Fig. 6). Some mutant mice exhibited a complete uncoupling of atrial and ventricular rhythms (third-degree block), which demonstrates that I_f activity is also critical for impulse conduction through the AVN. Consistent with the prominent effect of hHCN4-AYA expression in pacemaking of PF myocytes, mutant mice showed a significantly (19%) prolonged QRS complex. Some mutant mice exhibited ventricular extrasystoles and episodes of ventricular tachycardia (Fig.9). Like SAN, both mutant AVN and PF myocytes showed a high incidence of DADs. These DADs may underlie AVBs by preventing AVN activation and inducing ventricular extrasystoles and tachycardia. In this context, modeling studies suggest that a limited number of myocytes developing synchronous DADs is sufficient to trigger premature ventricular contraction and arrhythmia in PF[57]. Our observation of ventricular arrhythmia in mutant mice is compatible with a previous case report showing ventricular tachycardia in a patient with a genetic loss-of-function of *HCN4*[20]. Since HCN3 channels have been proposed to regulate ventricular repolarization[58], mutant hHCN4-AYA channels may also induce arrhythmogenic DADs in ventricular myocytes by exerting a dominant-negative effect on native HCN3 subunits.

In contrast to what was reported in cardiac-specific *HCN4* knockout mice (ci-HCN4-KO)[23], we did not observe lethal heart block in mutant mice. In mutant mice with complete AV block, a viable ventricular idiopathic rhythm persisted, suggesting that the His-Purkinje network was still able to generate sufficient automaticity in spite of I_f silencing. Both Baruscotti and coworkers[23] and our group used α-MHC promoter lines. It is thus unlikely that the difference between ciHCN4-KO and HCN4-AYA mutant mice is due to differential efficiency of *Cre*-mediated inactivation of *HCN4* alleles[23] versus expression of hHCN4-AYA transgene in the conduction system described here. It is possible, though, that idioventricular rhythm deficiency in ci-HCN4-KO mice is a consequence of a fast *Cre*–mediated loss of HCN4 protein versus more slowly progressing hHCN4-AYA –mediated I_f silencing in mutant mice. Another hypothesis is that idioventricular rhythm requires intact HCN4 protein. We did not observe atrioventricular dysfunction in control mice treated with ivabradine. We hypothesize that ivabradine does not impair impulse conduction because of

its use-dependent properties of block, which predicts that the drug dissociates from f-channels at low SAN beating rates[59].

Genetic inactivation of I_{KACh} by *GIRK4* gene knockout effectively prevented SAN pauses, AVBs, and ventricular tachycardia in mutant mice (Fig. 9). I_{KACh} slows diastolic depolarization[60] and atrioventricular conduction[61] in the mouse heart. Since the membrane voltage of mutant pacemaking myocytes is characterized by slow diastolic depolarization and a high incidence of DADs, it is tempting to speculate that I_{KACh} activation favors DAD formation in mutant mice *in vivo*. In contrast, in the absence of I_{KACh}, a significant fraction of DADs would elicit a normal action potential in Mut/*GIRK4*$^{-/-}$ mice, thus abolishing SAN pauses and facilitating AVN activation and conduction. The improved SAN activity and impulse conduction in turn may suppress arrhythmogenic DADs in PFs of Mut/*GIRK4*$^{-/-}$ mice. The presence of such a mechanism is supported by the observation that the vast majority of episodes of ventricular tachycardia are preceded by SAN pauses or AVBs (Fig. 9). In addition, PF myocytes may develop fully conducted action potentials rather than arrhythmogenic DADs in the absence of I_{KACh} *in vivo*.

Our results demonstrate that I_f is an important mechanism effective in counterbalancing the negative dromotropic effect of I_{KACh} activation in AVN, and show that f-channels provide AVN myocytes with a critical inward current under physiological conditions. It is an interesting observation that both mutant and Mut/*GIRK4*$^{-/-}$ mice show a preserved degree of heart rate regulation, as well as normal recovery of resting heart rate (Supplementary Fig. 8). This last observation suggests that the delayed recovery of the resting heart rate, which is typically present in *GIRK4*$^{-/-}$[60] mice, is linked to I_f activity. It is an attractive hypothesis that pharmacological inhibition of GIRK4 channels in the heart may be used to restore atrioventricular dysfunction in patients with atrioventricular block due to loss-of-function of ion channels involved in cardiac conduction.

Materials and methods

Cloning of HCN constructs

Murine HCN4 and HCN2 (mHCN4 and mHCN2) and human HCN4 (hHCN4) cDNAs (GenBank Acc. NM_001081192, NM_008226, and NM_005477) in pCDNA1 vector were kindly provided by Benjamin Kaupp (Forschungszentrum caesar, Bonn, Germany). A hemagglutinin (HA) epitope tag (YPYDVPDYA) was attached to the N-terminus of the open reading frame of hHCN4[19]. The selectivity filter GYG motif was mutated to AYA by overlap PCR-based, site-directed mutagenesis resulting in hHCN4-G480A/G482A (hHCN4-AYA). For two-electrode voltage-clamp experiments mHCN4, mHCN2, and HA-hHCN4-AYA were cloned into an RNA expression vector (pGem-HeJuel[62]). For the generation of transgenic mice, the Tet-responsive element (Tre-Tight) of pTRE-Tight (Clontech, Mountain View, CA, USA) was cloned into pWHERE2 v.01 (Invivogen, San Diego, CA, USA). HA-hHCN4-AYA was inserted downstream of Tre. All coding sequences were verified by direct sequencing.

Two-electrode voltage-clamp experiments in *Xenopus* oocytes

Xenopus oocytes were obtained from tricaine-anesthetized animals. Ovaries were treated with collagenase (3 mg/ml, Sigma-Aldrich Chemie GmbH, Taufkirchen, Germany) in OR2 solution (in mM: NaCl 82.5, KCl 2, $MgCl_2$ 1, HEPES 5, pH 7.4) for 2–3 h, and subsequently stored in gentamycin solution (in mM: NaCl 75, KCl 2, $CaCl_2$ 2, $MgCl_2$ 1, HEPES 5, pH 7.4) with additional Na pyruvate (550 mg/l) and gentamycin (50 mg/l) at 18 °C. Oocytes were injected with cRNA (in ng)-encoding mHCN4 (1.0 or 0.5), mHCN2 (0.2 or 0.1), and HA-hHCN4-AYA (1.0 or 0.2). The effect of HA-hHCN4-AYA on mHCN4 and mHCN2 was tested by coexpression of the two constructs with the pore mutant at a 1:1 ratio. Standard two-electrode voltage-clamp recordings were performed at room temperature (21–23 °C) three days after injection. ND66 solution (in mM: NaCl 66, KCl 32, $CaCl_2$ 1.8, $MgCl_2$ 1, HEPES 5, pH 7.4) was used as a perfusion solution[63]. The pipette solution contained 3 M KCl.

Generation of mutant transgenic mice

Transgenic mice carrying the pWHERE-Tre-HA-hHCN4-AYA (C57BL/6J-Tg(tetO-hHCN4-AYA) CIsb) construct were generated by pronuclear injection using standard techniques. Founder mice and the resulting offspring were genotyped by PCR (primers: 5′ – GGCATGTCCGACGTCTGGCTCAC – 3′ and 5′ – TCACGAAGTTGGGGTCCGCATTGG – 3′) using ear or tail biopsies and crossed with heart-specific promoter transgenic mice (C57BL/6J -Tg(Myh6-tTA)6Smbf/J)[25], which were obtained from the Jackson Laboratories (Bar Harbor, MA, USA) and backcrossed to the C57BL/6J background for more than seven generations. These mice are referred to as mutant (Mut) mice. To investigate the consequences of I_f silencing in Purkinje fiber cells, mutant mice (C57BL/6J-Tg(Myh6-tTA, tetO-hHCN4-AYA) were crossed with heterozygous knock-in mice in which EGFP was knocked in the gene coding for Cx40 ($Cx40^{+/tm(EGFP)Lumi}$)[31] to give rise to triple-transgenic C57BL/6J-Tg(Myh6-tTA, tetO-hHCN4-AYA, $Cx40^{+/tm(EGFP)}$ (short: Mut/$Cx40^{+/EGFP}$) mice. To generate double-transgenic mutant mice that are also GIRK4 deficient (Mut/$GIRK4^{-/-}$, double-transgenic mutant mice were crossbred with $GIRK4^{-/-}$ mice[37].

Care and use of animals

Mixed genotype groups of each gender of no more than five animals were housed in standard mouse cages under specific pathogen-free conditions (12:12-h dark-light cycle, constant temperature, constant humidity, and food and water *ad libitum*). Double-transgenic mutant mice and their tTA transgenic control littermates received either normal food or food drugged with 50 mg/kg doxycycline hydrochloride (Ssniff Spezialdiäten, Soest, Germany; Graymor Chemical, Hamburg, Germany) when breeding pairs were set up.

Care and use of animals and experimental procedures were in accordance with the German Law for the Protection of Animals and approved by the Ministry of Science and Public Health of the City State of Hamburg, Germany. The study conforms to the *Guide for the Care and Use of Laboratory Animals* published by the US National Institutes of Health (NIH Publication No. 85-23, revised 1996), and to European directives (86/609/CEE).

Protein isolation and Western blot

Frozen hearts from 10-week-old male mice were pulverized in liquid nitrogen and homogenized in 10% glycerol, 3% SDS, and 62.5 mM Tris (pH 6.8) containing a protease inhibitor mix (Sigma-Aldrich Chemie GmbH, Taufkirchen, Germany). Proteins were fractionated on NuPAGE• 4–12% Bis-Tris gels (Invitrogen) in NuPAGE• MOPS SDS running buffer (Invitrogen) and electrophoretically transferred to PROTRAN• nitrocellulose membranes (Whatman GmbH, Dassel, Germany). Western blot analysis was performed according to standard methods. Antibodies against the HA epitope tag (3F10 (Roche, Basel, Switzerland), 1:500 dilution) and calsequestrin (Affinity BioReagents, Golden, CO, USA) 1:2500 dilution) were used as primary antibodies.

Staining of intact SAN-AVN preparations and isolated myocytes

Whole-mount immunofluorescence: Mouse heart nodal tissue was dissected from the right atrium including the SAN and AVN regions and fixed at 4°C for 20 min with 4% paraformaldehyde. Fixed tissue was washed for 30 min in PBS at 4°C and incubated for 30 min with 10% goat serum and 1% mouse blocking reagent (Vectashield) in PBS/0.1% TritonX100. Subsequent incubation with primary antibodies was carried out overnight at 4°C in mouse monoclonal anti-HA (1/100, clone 12C5A, DSHB Univ. Iowa) and rabbit polyclonal anti-HCN4 (1/200, Alomone), or anti rabbit HCN1 (1/200, Alomone) diluted in PBS/0.1% TritonX100. After rinse in PBS-TX100, tissue was further incubated at 37°C for 1 hour using a 1/100 dilution of secondary Alexa488-conjugated anti-mouse IgGs and Alexa555-conjugated anti-rabbit IgGs, both from Molecular Probes (InVitrogen, Saint Aubin, France). After rinse with PBS/TritonX100, tissue was briefly treated with Sudan Black (Sigma, 3% in 70% ethanol) to quench autofluorescence, and sequentially washed in 70% ethanol and water before mounting it for photomicroscopy with an EOS Canon camera on a DMR1 Leica upright microscope equipped with 5X and 16X lenses. Enzymatically dissociated SAN myocytes were placed into chambers and allowed to attach to Cell-Tak coated wells (3.5 μg/cm2) for 1 hr (LAB-TEK II Chamber Slide, NUNC). Cells were then fixed with 4% paraformaldehyde for 20 minutes at room temperature (RT), followed by soaking in 1xPBS for several hours. 250 μl of 2% Bovine Serum Albumin (Sigma) containing mouse anti HCN4 monoclonal antibody (Neuromab, 1:100), rat anti HA monoclonal (Roche, 1:250) were added and allowed to incubate overnight at 4 degrees in a humid chamber. Cells were rinsed for 4 × 15 minutes (1xPBS). Goat anti-rat FITC secondary (Molecular Probes, 1:500), donkey anti mouse Alexa-647 (Molecular Probes, 1:500) and DAPI were incubated for 90 minutes at RT followed by 4×15 minutes (1xPBS). Prolong gold (Invitrogen) was overlayed and a glass coverslip gently placed over the sample. Images were taken with a Leica confocal microscope (Leica SPE). Image analysis was carried out on Metamorph Image Analysis software.

Isolation of SAN, AVN, and PF cells

SAN and AVN myocytes were isolated from control and mutant mice, and individual PF cells were isolated from Mut/*Cx40*$^{eGFP/+}$ mice as follows[31,32]:

Hearts were removed under general anesthesia using 10 mg/kg of xylazine (Rompun 2%, Bayer AG, Leverkusen, Germany) and 100 mg/kg of ketamine (Imalgène, Merial,

Bourgelat, France). The SAN and AVN regions, as well as the endocardial ventricular tissue, were excised in pre-warmed (35 °C) Tyrode's solution containing (in mM): NaCl 140, KCl 5.4, $CaCl_2$ 1.8, $MgCl_2$ 1, HEPES-NaOH 5, and D-glucose 5.5 (adjusted to pH=7.4 with NaOH). Tissue strips were then transferred into a "low-Ca^{2+}-low-Mg^{2+}" solution containing (in mM): NaCl 140, KCl 5.4, $MgCl_2$ 0.5, $CaCl_2$ 0.2, KH_2PO_4 1.2, taurine 50, D-glucose 5.5, bovine serum albumin (BSA), 1 mg/ml; HEPES-NaOH 5 (adjusted to pH=6.9 with NaOH). Tissue was digested by Liberase TH (229 U/ml, Roche, Boulogne-Billancourt, France), elastase (1.9 U/ml, Boehringer, Mannheim, Germany), and 200 μM $CaCl_2$. Digestion was carried out under manual mechanical agitation at 35 °C for 9–13 min. Tissue strips were then washed and transferred into a modified "Kraftbrühe" (KB) medium containing (in mM): L-glutamic acid 70, KCl 20, KOH 80, (±)D-β-OH-butyric acid10, KH_2PO_4 10, taurine 10, BSA 1mg/ml, and HEPES-KOH 10 (adjusted to pH=7.4 with KOH). Single SAN, AVN, and PF cells were then isolated by agitation in KB solution at 35 °C. Cellular automaticity was restored by re-adapting the cells to a physiological extracellular Ca^{2+}concentration by addition of a solution containing (in mM): NaCl 10, $CaCl_2$ 1.8, and normal Tyrode's solution containing BSA (1 mg/ml). The final cell storage solution contained (mM): NaCl 100, KCl 35, $CaCl_2$ 1.3, $MgCl_2$ 0.7, L-glutamic acid 14, (±)D-β-OH-butyric acid 2, KH_2PO_4 2, taurine 2, BSA 1mg/ml (pH=7.4), and gentamycin (50 μg/ml). All chemicals were from SIGMA (St. Quentin Fallavier, France).

Patch-clamp recordings of mouse SAN, AVN, and PF cells

The basal extracellular Tyrode's solution used in all recordings contained (in mM): NaCl 140, KCl 5.4, $CaCl_2$ 1.8, $MgCl_2$ 1.0, HEPES-NaOH 5.0, and D-glucose 5.5 (adjusted to pH 7.4 with NaOH). Automaticity was recorded by the perforated patch-clamp technique using escin (30 μM); I_f was recorded under standard whole-cell configuration. Patch-clamp electrodes had a resistance of 4–5 MΩ when filled with an intracellular solution containing (mM): K^+-aspartate 130, NaCl 10.0, ATP-Na^+ salt 2.0, creatine phosphate 6.6, GTP-Mg^{2+} 0.1, $CaCl_2$ 0.04 (pCa=7.0), HEPES-KOH 10.0 (adjusted to pH=7.2 with KOH). All experiments were carried out at 36 °C. All electrophysiological data were recorded and analyzed using pCLAMP 9.2 (Molecular Devices, St. Grégoire, France). All chemicals were from SIGMA (St. Quentin Fallavier, France).

Ca^{2+} imaging and analysis of LCRs

Spontaneous $[Ca^{2+}]_i$ transients and LCRs were recorded in SAN pacemaker myocytes loaded with Fluo-4 AM (20 μM, 35 minutes) at 36°C. Images were obtained with confocal microscopy (Zeiss LSM 780) by scanning the myocyte with an Argon laser in line scan configuration (3.78 ms and/or 1.53 ms line rate); fluorescence was excited at 488 nm and emissions were collected at >505 nm. A 63× oil immersion objective were used to record $[Ca^{2+}]_i$ in isolated SAN myocytes. Image analyses were performed by ImageJ software. Images were corrected for the background fluorescence and the fluorescence values (F) were normalized to the basal fluorescence (F0) to obtain the fluorescence ratio (F/F0). Integrals of light intensity were analyzed by pCLAMP 9.2 (Molecular Devices, St. Grégoire, France). $[Ca^{2+}]_i$ parameters were analyzed as follow: upstroke velocity of $[Ca^{2+}]_i$ transient was measured from the threshold to the peak of the $[Ca^{2+}]_i$ transient; $[Ca^{2+}]_i$ transient duration was measured from the threshold of $[Ca^{2+}]_i$ transients to 90% decay; $[Ca^{2+}]_i$ transient

recovery time was measured from the peak of the $[Ca^{2+}]_i$ transient to 90% decay. Image acquisition and analysis were performed on workstations of the Montpellier RIO Imaging facility.

Measurements in isolated right atria

The spontaneous beat frequency and its regulation in isolated atrial preparation from control and mutant mice were recorded in thermostated organ baths as described previously[64]. Effects of pharmacological activation of sympathetic function on heart rate response were examined by adding the adrenoceptor agonist isoproterenol at cumulatively increasing concentrations (ISO, 0.001-1.0 μM). Effects of pharmacological blockade of I_f were investigated by adding 0.3–1.0 μM ivabradine (IVA).

Telemetric recordings of ECG and analysis

For telemetric ECG recordings, adult male mice were anesthetized with 2% isoflurane. A midline incision was made on the back along the spine to insert a telemetric transmitter (TA10EA-F20, Data Sciences International, 's-Hertogenbosch, The Netherland) into a subcutaneous pocket with paired wire electrodes placed over the thorax (chest bipolar ECG lead). Local anesthesia was performed with lidocaine (1%) injected subcutaneously at the sites of electrodes and transmitter implantation. To manage possible post-surgery pain, Advil (paracetamol and ibuprofen, 7 mL/l) was added to the drinking water for four days after implantation. Experiments were initiated at least 8 days after recovery from surgical implantation. Mice were housed in individual cages with *ad libitum* access to food and water and were exposed to standard 12-h light/dark cycles in a thermostatically controlled room. ECG signals were recorded using a telemetry receiver and an analog-to-digital conversion data acquisition system for display and analysis by Dataquest A.R.T.™ software. Heart rates were determined from interbeat (RR) intervals of the ECG. Mean heart rate values were obtained from each mouse for a 24-h period. For drug administration or exercise experiments, mean heart rate values were calculated in each mouse by analyzing different periods of 5 min. ECG parameters were measured with ECG Auto 1.5.7 software (EMKA, Paris, France). Swimming tests were performed using customized Plexiglas boxes (15×32×13 cm (WxLxH)) filled with pre-warmed water (32°C).

Telemetric blood pressure recordings

Mice with a body weight of >24 g were anesthetized by i.p. administration of ketamine/xylazine adapted to body weight. Telemetric transmitters (Physiotel PA-C10, Data Sciences International) were subcutaneously implanted with the sensing tip placed in the aorta via the left carotid artery. After 10 days of recovery from surgery, interventions and recordings (Dataquest A.R.T.™ software for acquisition and analysis) were started. For each mouse, blood pressure was continuously recorded for at least 48 h. For data analysis, mean blood pressure data were obtained for each consecutive minute within one recording period. The blood pressure mean data were then sorted by the corresponding activity in 7 bins between "0" (no activity) and "7" (activity >30 arbitrary units (aU)) and averaged over all mice.

Data analysis

Results are presented as means ± the standard error of the mean (S.E.M.). Statistical significance was defined as $p<0.05$. Statistical tests used in each experiment are specified throughout the figure legends. Analysis was performed using Prism v6 (GraphPad Software).

Supplementary Material

Refer to Web version on PubMed Central for supplementary material.

Acknowledgments

We thank I. Hermans-Borgmeyer for transgenic services, K. Sauter for technical assistance, and the teams of the UKE animal facility (Hamburg) of the RAM animal facility (Montpellier) for animal care. We also thank N. Lamb for helpful discussions. The project was supported by the *Agence Nationale pour la Recherche* grant ANR-06-PHISIO-004-01, ANR-2010-BLAN-1128-01, ANR-09-GENO-034, and ANR-13-BSV1-0023-02, the NIH R01HL087120-A2 grant (M.M.), the *Fondation de France* grant 2008002730 (J. N.), the *Fondation pour la Recherche Medicale* grant DPC20111122986 (A.F.), by the Deutsche Forschungsgemeinschaft Grant IS63/1–1/2 (to D.I. and H.E), IS63/3-1/2 (D.I.), and DFG FOR 604 and Es 88/10-1 (T.E.). P.M. was supported by the CavNet, a Research Training Network (RTN) funded through the European Union Research Programme (6FP) MRTN-CT-2006-035367. L.M. is a recipient of a postdoctoral fellowship by the *Fondation Lefoulon-Delalande*. The authors wish to thank the Montpellier RIO Imaging facility and their financing bodies. The IGF group is a member of the Laboratory of Excellence « Ion Channel Science and Therapeutics » supported by a grant from ANR (ANR-11-LABX-0015).

References

1. Mangoni ME, Nargeot J. Genesis and regulation of the heart automaticity. Physiol Rev. 2008; 88:919–982. [PubMed: 18626064]
2. Benditt, DG., et al. Sinus node dysfunction: pathophysiology, clinical features, evaluation and treatment. In: Zipes, DP.; Jalife, J., editors. Cardiac Electrophysiology, From Cell to Bedside. Philadelphia: W.B. Saunders Company; 1995. p. 1215-1247.
3. Mangrum JM, DiMarco JP. The evaluation and management of bradycardia. N Engl J Med. 2000; 342:703–709. [PubMed: 10706901]
4. Bertram H, Paul T, Beyer F, Kallfelz HC. Familial idiopathic atrial fibrillation with bradyarrhythmia. Eur J Pediatr. 1996; 155:7–10. [PubMed: 8750801]
5. Dobrzynski H, Boyett MR, Anderson RH. New insights into pacemaker activity: promoting understanding of sick sinus syndrome. Circulation. 2007; 115:1921–1932. [PubMed: 17420362]
6. Gillis AM, et al. HRS/ACCF expert consensus statement on pacemaker device and mode selection. Developed in partnership between the Heart Rhythm Society (HRS) and the American College of Cardiology Foundation (ACCF) and in collaboration with the Society of Thoracic Surgeons. Heart Rhythm. 2012; 9:1344–1365. [PubMed: 22858114]
7. DiFrancesco D. Pacemaker mechanisms in cardiac tissue. Annu Rev Physiol. 1993; 55:455–472. [PubMed: 7682045]
8. DiFrancesco D. The role of the funny current in pacemaker activity. Circ Res. 2010; 106:434–446. [PubMed: 20167941]
9. Lakatta EG, DiFrancesco D. What keeps us ticking: a funny current, a calcium clock, or both? J Mol Cell Cardiol. 2009; 47:157–170. [PubMed: 19361514]
10. Ludwig A, Zong X, Jeglitsch M, Hofmann F, Biel M. A family of hyperpolarization-activated mammalian cation channels. Nature. 1998; 393:587–591. [PubMed: 9634236]
11. Santoro B, et al. Identification of a gene encoding a hyperpolarization-activated pacemaker channel of brain. Cell. 1998; 93:717–729. [PubMed: 9630217]

12. Ishii TM, Takano M, Xie LH, Noma A, Ohmori H. Molecular characterization of the hyperpolarization-activated cation channel in rabbit heart sinoatrial node. J Biol Chem. 1999; 274:12835–12839. [PubMed: 10212270]
13. Seifert R, et al. Molecular characterization of a slowly gating human hyperpolarization-activated channel predominantly expressed in thalamus, heart, and testis. Proc Natl Acad Sci U S A. 1999; 96:9391–9396. [PubMed: 10430953]
14. Herrmann S, Layh B, Ludwig A. Novel insights into the distribution of cardiac HCN channels: An expression study in the mouse heart. J Mol Cell Cardiol. 2011; 51:997–1006. [PubMed: 21945247]
15. Fenske S, et al. Sick sinus syndrome in HCN1-deficient mice. Circulation. 2013; 128:2585–2594. [PubMed: 24218458]
16. Milanesi R, Baruscotti M, Gnecchi-Ruscone T, DiFrancesco D. Familial sinus bradycardia associated with a mutation in the cardiac pacemaker channel. N Engl J Med. 2006; 354:151–157. [PubMed: 16407510]
17. Nof E, et al. Point mutation in the HCN4 cardiac ion channel pore affecting synthesis, trafficking, and functional expression is associated with familial asymptomatic sinus bradycardia. Circulation. 2007; 116:463–470. [PubMed: 17646576]
18. Schweizer PA, et al. cAMP sensitivity of HCN pacemaker channels determines basal heart rate but is not critical for autonomic rate control. Circ Arrhythm Electrophysiol. 2010; 3:542–552. [PubMed: 20693575]
19. Schulze-Bahr E, et al. Pacemaker channel dysfunction in a patient with sinus node disease. J Clin Invest. 2003; 111:1537–1545. [PubMed: 12750403]
20. Ueda K, et al. Functional characterization of a trafficking-defective HCN4 mutation, D553N, associated with cardiac arrhythmia. J Biol Chem. 2004; 279:27194–27198. [PubMed: 15123648]
21. Herrmann S, Stieber J, Stockl G, Hofmann F, Ludwig A. HCN4 provides a 'depolarization reserve' and is not required for heart rate acceleration in mice. Embo J. 2007; 26:4423–4432. [PubMed: 17914461]
22. Hoesl E, et al. Tamoxifen-inducible gene deletion in the cardiac conduction system. J Mol Cell Cardiol. 2008; 45:62–69. [PubMed: 18538341]
23. Baruscotti M, et al. Deep bradycardia and heart block caused by inducible cardiac-specific knockout of the pacemaker channel gene Hcn4. Proc Natl Acad Sci U S A. 2011; 108:1705–1710. [PubMed: 21220308]
24. Gossen M, Bujard H. Tight control of gene expression in mammalian cells by tetracycline-responsive promoters. Proc Natl Acad Sci U S A. 1992; 89:5547–5551. [PubMed: 1319065]
25. Yu Z, Redfern CS, Fishman GI. Conditional transgene expression in the heart. Circ Res. 1996; 79:691–697. [PubMed: 8831492]
26. Stieber J, et al. The hyperpolarization-activated channel HCN4 is required for the generation of pacemaker action potentials in the embryonic heart. Proc Natl Acad Sci U S A. 2003; 100:15235–15240. [PubMed: 14657344]
27. Verheijck EE, et al. Electrophysiological features of the mouse sinoatrial node in relation to connexin distribution. Cardiovasc Res. 2001; 52:40–50. [PubMed: 11557232]
28. Liu J, Dobrzynski H, Yanni J, Boyett MR, Lei M. Organisation of the mouse sinoatrial node: structure and expression of HCN channels. Cardiovasc Res. 2007; 73:729–738. [PubMed: 17222809]
29. Mangoni ME, Nargeot J. Properties of the hyperpolarization-activated current (I_f) in isolated mouse sino-atrial cells. Cardiovasc Res. 2001; 52:51–64. [PubMed: 11557233]
30. DiFrancesco D, Ferroni A, Mazzanti M, Tromba C. Properties of the hyperpolarizing-activated current (i_f) in cells isolated from the rabbit sino-atrial node. J Physiol. 1986; 377:61–88. [PubMed: 2432247]
31. Miquerol L, et al. Architectural and functional asymmetry of the His-Purkinje system of the murine heart. Cardiovasc Res. 2004; 63:77–86. [PubMed: 15194464]
32. Marger L, et al. Pacemaker activity and ionic currents in mouse atrioventricular node cells. Channels (Austin). 2011; 5:241–250. [PubMed: 21406959]
33. Bers DM. Calcium and cardiac rhythms: physiological and pathophysiological. Circ Res. 2002; 90:14–17. [PubMed: 11786512]

34. Bers DM. Cardiac sarcoplasmic reticulum calcium leak: basis and roles in cardiac dysfunction. Annu Rev Physiol. 2014; 76:107–127. [PubMed: 24245942]
35. Sah VP, et al. Cardiac-specific overexpression of RhoA results in sinus and atrioventricular nodal dysfunction and contractile failure. J Clin Invest. 1999; 103:1627–1634. [PubMed: 10377168]
36. Bois P, Bescond J, Renaudon B, Lenfant J. Mode of action of bradycardic agent, S 16257, on ionic currents of rabbit sinoatrial node cells. Br J Pharmacol. 1996; 118:1051–1057. [PubMed: 8799581]
37. Wickman K, Nemec J, Gendler SJ, Clapham DE. Abnormal heart rate regulation in *GIRK4* knockout mice. Neuron. 1998; 20:103–114. [PubMed: 9459446]
38. Monfredi O, Maltsev VA, Lakatta EG. Modern concepts concerning the origin of the heartbeat. Physiology (Bethesda). 2013; 28:74–92. [PubMed: 23455768]
39. Ragueneau I, et al. Pharmacokinetic-pharmacodynamic modeling of the effects of ivabradine, a direct sinus node inhibitor, on heart rate in healthy volunteers. Clin Pharmacol Ther. 1998; 64:192–203. [PubMed: 9728900]
40. Ludwig A, et al. Absence epilepsy and sinus dysrhythmia in mice lacking the pacemaker channel HCN2. Embo J. 2003; 22:216–224. [PubMed: 12514127]
41. Herrmann S, Fabritz L, Layh B, Kirchhof P, Ludwig A. Insights into sick sinus syndrome from an inducible mouse model. Cardiovasc Res. 2011; 90:38–48. [PubMed: 21193513]
42. Zhang Q, et al. Functional roles of a Ca^{2+}-activated K^+ channel in atrioventricular nodes. Circ Res. 2008; 102:465–471. [PubMed: 18096820]
43. Weisbrod D, et al. SK4 Ca^{2+} activated K^+ channel is a critical player in cardiac pacemaker derived from human embryonic stem cells. Proc Natl Acad Sci U S A. 2013; 110:E1685–E1694. [PubMed: 23589888]
44. Mangoni ME, et al. Functional role of L-type Cav1.3 Ca^{2+} channels in cardiac pacemaker activity. Proc Natl Acad Sci U S A. 2003; 100:5543–5548. [PubMed: 12700358]
45. Clark RB, et al. A rapidly activating delayed rectifier K^+ current regulates pacemaker activity in adult mouse sinoatrial node cells. Am J Physiol Heart Circ Physiol. 2004; 286:H1757–H1766. [PubMed: 14693686]
46. Bers DM. Calcium cycling and signaling in cardiac myocytes. Annu Rev Physiol. 2008; 70:23–49. [PubMed: 17988210]
47. Neco P, et al. Paradoxical effect of increased diastolic Ca2+ release and decreased sinoatrial node activity in a mouse model of catecholaminergic polymorphic ventricular tachycardia. Circulation. 2012; 126:392–401. [PubMed: 22711277]
48. Vinogradova TM, et al. Sarcoplasmic Reticulum Ca^{2+} Pumping Kinetics Regulates Timing of Local Ca^{2+} Releases and Spontaneous Beating Rate of Rabbit Sinoatrial Node Pacemaker Cells. Circ Res. 2010; 107:767–775. [PubMed: 20651285]
49. Rigg L, Heath BM, Cui Y, Terrar DA. Localisation and functional significance of ryanodine receptors during beta-adrenoceptor stimulation in the guinea-pig sino-atrial node. Cardiovasc Res. 2000; 48:254–264. [PubMed: 11054472]
50. Vinogradova TM, Bogdanov KY, Lakatta EG. beta-Adrenergic stimulation modulates ryanodine receptor Ca^{2+} release during diastolic depolarization to accelerate pacemaker activity in rabbit sinoatrial nodal cells. Circ Res. 2002; 90:73–79. [PubMed: 11786521]
51. Wu Y, et al. Calmodulin kinase II is required for fight or flight sinoatrial node physiology. Proc Natl Acad Sci U S A. 2009; 106:5972–5977. [PubMed: 19276108]
52. Alig J, et al. Control of heart rate by cAMP sensitivity of HCN channels. Proc Natl Acad Sci U S A. 2009; 106:12189–12194. [PubMed: 19570998]
53. Kohl P, Noble D. Mechanosensitive connective tissue: potential influence on heart rhythm. Cardiovasc Res. 1996; 32:62–68. [PubMed: 8776404]
54. Boyett MR, Honjo H, Kodama I. The sinoatrial node, a heterogeneous pacemaker structure. Cardiovasc Res. 2000; 47:658–687. [PubMed: 10974216]
55. Nikmaram MR, Boyett MR, Kodama I, Suzuki R, Honjo H. Variation in effects of Cs^+, UL-FS-49, and ZD-7288 within sinoatrial node. Am J Physiol. 1997; 272:H2782–H2792. [PubMed: 9227558]

56. Joung B, et al. Delayed afterdepolarization in intact canine sinoatrial node as a novel mechanism for atrial arrhythmia. J Cardiovasc Electrophysiol. 2011; 22:448–454. [PubMed: 21040091]
57. Xie Y, Sato D, Garfinkel A, Qu Z, Weiss JN. So little source, so much sink: requirements for afterdepolarizations to propagate in tissue. Biophys J. 2010; 99:1408–1415. [PubMed: 20816052]
58. Fenske S, et al. HCN3 contributes to the ventricular action potential waveform in the murine heart. Circ Res. 2011; 109:1015–1023. [PubMed: 21903939]
59. Bucchi A, Baruscotti M, DiFrancesco D. Current-dependent block of rabbit sino-atrial node I_f channels by ivabradine. J Gen Physiol. 2002; 120:1–13. [PubMed: 12084770]
60. Mesirca P, et al. The G-protein-gated K^+ channel, I_{KACh}, is required for regulation of pacemaker activity and recovery of resting heart rate after sympathetic stimulation. J Gen Physiol. 2013; 142:113–126. [PubMed: 23858001]
61. Drici MD, Diochot S, Terrenoire C, Romey G, Lazdunski M. The bee venom peptide tertiapin underlines the role of I_{KACh} in acetylcholine-induced atrioventricular blocks. Br J Pharmacol. 2000; 131:569–577. [PubMed: 11015309]
62. Shih TM, Smith RD, Toro L, Goldin AL. High-level expression and detection of ion channels in Xenopus oocytes. Methods Enzymol. 1998; 293:529–556. [PubMed: 9711627]
63. Decher N, Bundis F, Vajna R, Steinmeyer K. KCNE2 modulates current amplitudes and activation kinetics of HCN4: influence of KCNE family members on HCN4 currents. Pflugers Arch. 2003; 446:633–640. [PubMed: 12856183]
64. Vandecasteele G, et al. Muscarinic and beta-adrenergic regulation of heart rate, force of contraction and calcium current is preserved in mice lacking endothelial nitric oxide synthase. Nat Med. 1999; 5:331–334. [PubMed: 10086391]

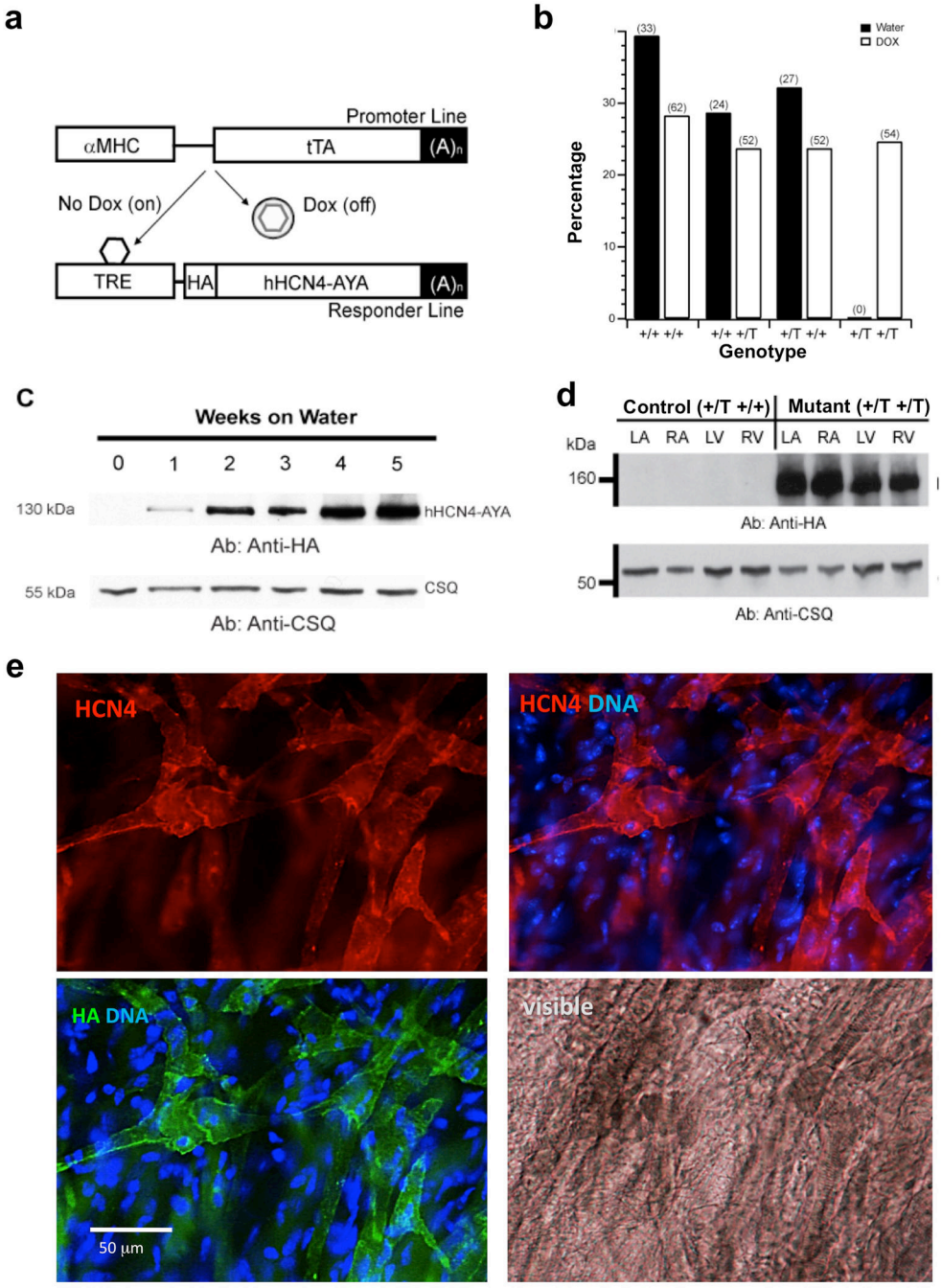

Figure 1. Generation of transgenic mutant mice

(**a**). Schematic illustration of the Tet-off system: The tetracycline-dependent transactivator (tTA) is expressed under the control of the alpha-myosin heavy chain (αMHC)-promoter. In the heart of double-transgenic (mutant) animals, tTA binds to the tetracycline responsive element (TRE), resulting in the expression of HA-hHCN4-AYA (hHCN4-AYA). A conformational change of tTA after the binding of doxycycline (DOX) inhibits transgene expression. (**b**) Percentage of genotypes obtained after breeding of the promoter line (first locus) and responder line (second locus) on water (black bars) or DOX (white bars).

Absolute animal numbers are given in parentheses above the bars. (**c**) Detection of transgenic hHCN4-AYA protein after 0 to 5 weeks after DOX withdrawal by Western blot. Total heart lysates were analyzed with antibodies against the HA-Tag and calsequestrin (CSQ). (**d**) Western blot analysis of protein isolated from the left atrium (LA), right atrium (RA), left ventricle (LV), and right ventricle (RV) of control and mutant mice. Different tissues lysates were analyzed with antibodies against the HA-Tag and CSQ. (**e**). Cellular expression of hHCN4-AYA protein in (N=4) SAN preparations (see Supplementary Fig. 2) isolated from mutant mice. Expression was evaluated by using anti-HCN4 (red, top-left panel) and anti-HA (green, bottom-left panel) antibodies. Staining of nuclei is shown in blue (top-right panel). Bottom-right panel: bright field image of tissue. Scale bar: 50 μm.

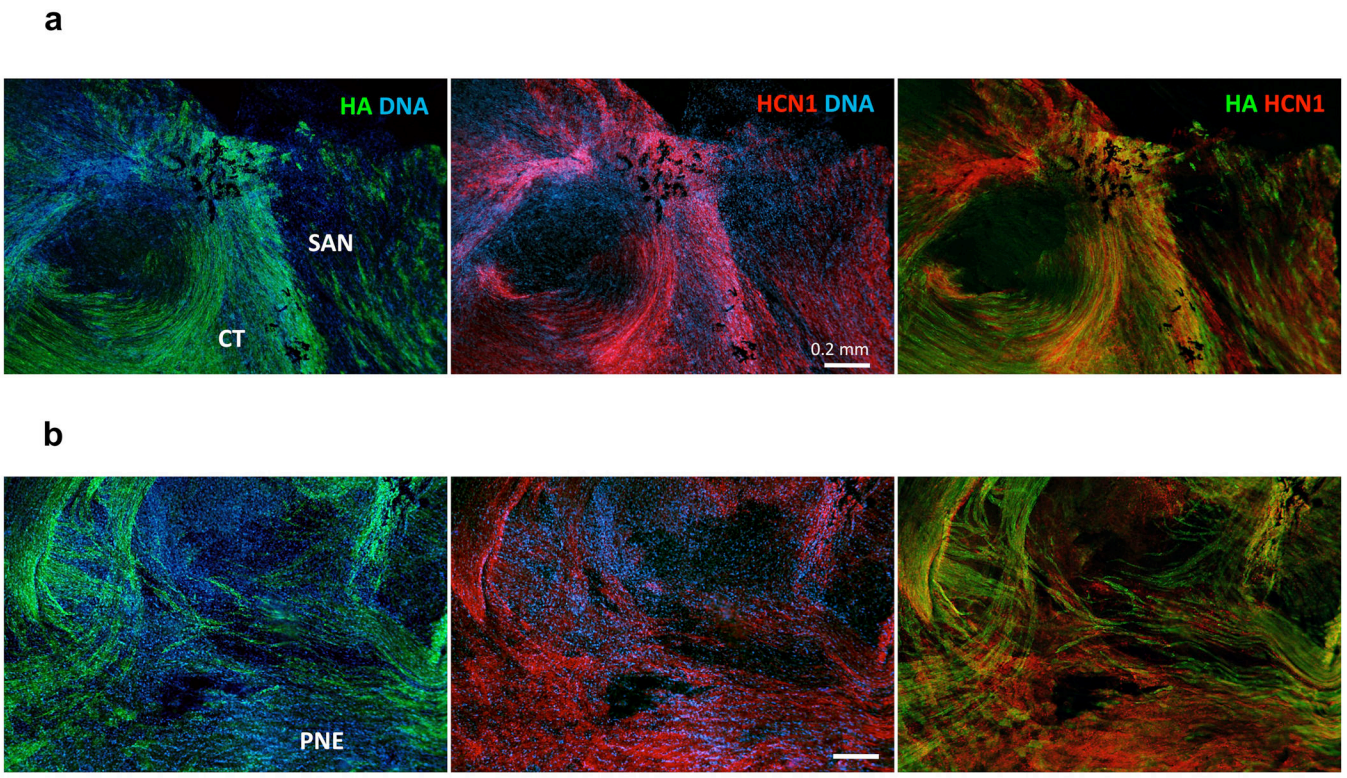

Figure 2. Transgene expression in the SAN and AVN regions of heart nodal tissues

Representative whole-mount stainings of n=4 mouse heart nodal tissues with close-up views of the mutant SAN (**a**) and AVN (**b**) regions stained with anti-HA (green) and anti-HCN1 (red) antibodies. Stainings of nuclei are shown in blue. See Supplementary Fig. 3 for the localization of the close-up views in whole-mount right atrial preparations containing the nodes. Scale bar: 100 μm.

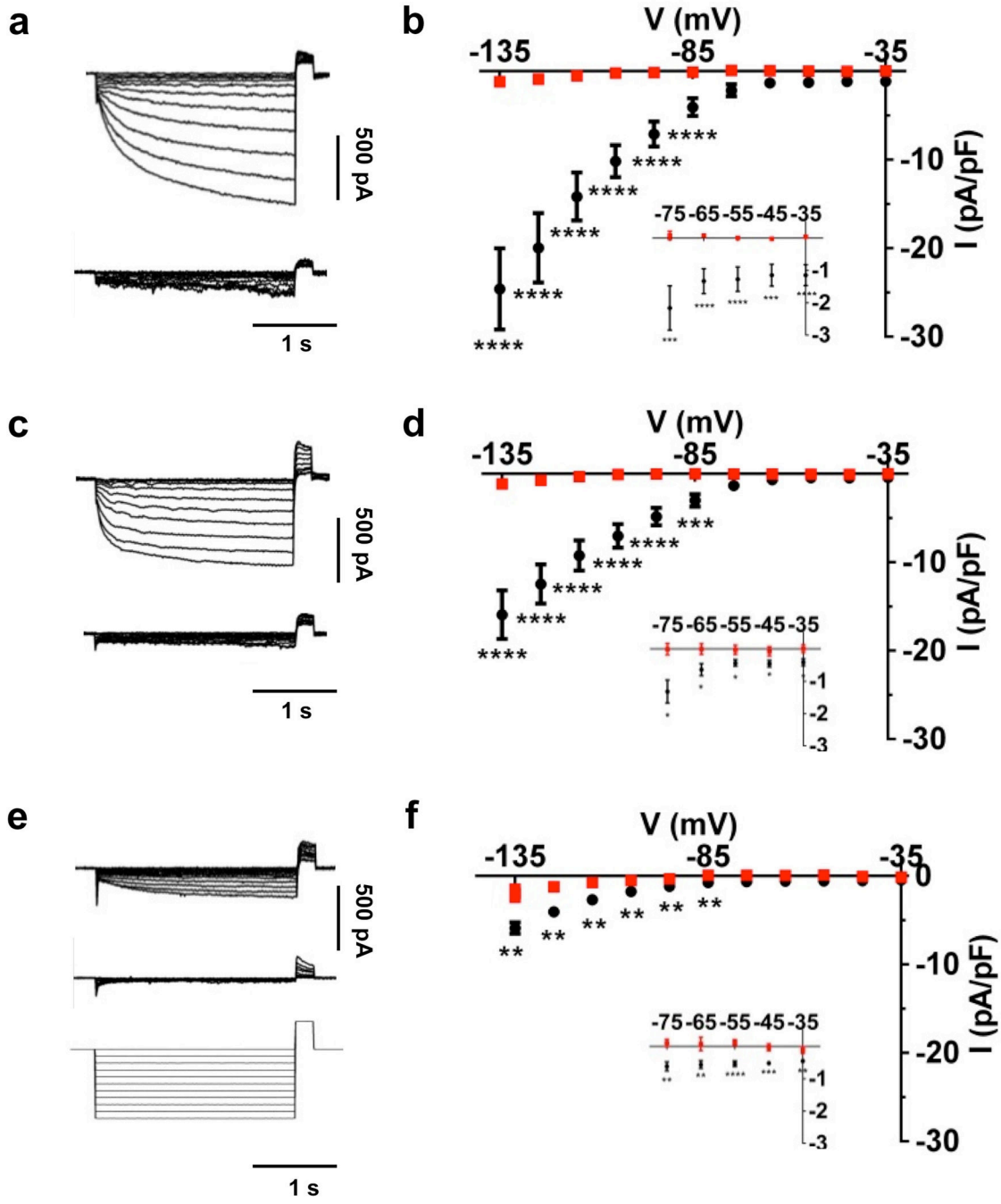

Figure 3. I_f in control and mutant pacemaker myocytes

Representative examples of I_f recordings (Cs^+-sensitive current, **a**) averaged current-to-voltage (I/V) curve (**b**) in control (n=11) and mutant (n=14) SAN pacemakers myocytes, (**c**) and (**d**) I_f recordings and I/V curve in AVN myocytes from control (n=16) and mutant (n=10) mice. (**e**) and (**f**) I_f recordings and I/V curve in myocytes from control (n=12) and mutant (n=9) PF myocytes. In (**a**), (**b**), and (**e**), the top panel shows I_f in control myocytes and the bottom panel shows I_f in mutant myocytes. In (**b**), (**d**), and (**f**), black circles indicate control and red squares indicate mutant myocytes. Statistical significance was tested at each

voltage using the unpaired *t*-test. *p<0.05, **p<0.01, ***p<0.001, ****p<0.0001. Error bars indicate S.E.M. The voltage-clamp protocol used for all the recordings is shown in (**e**).

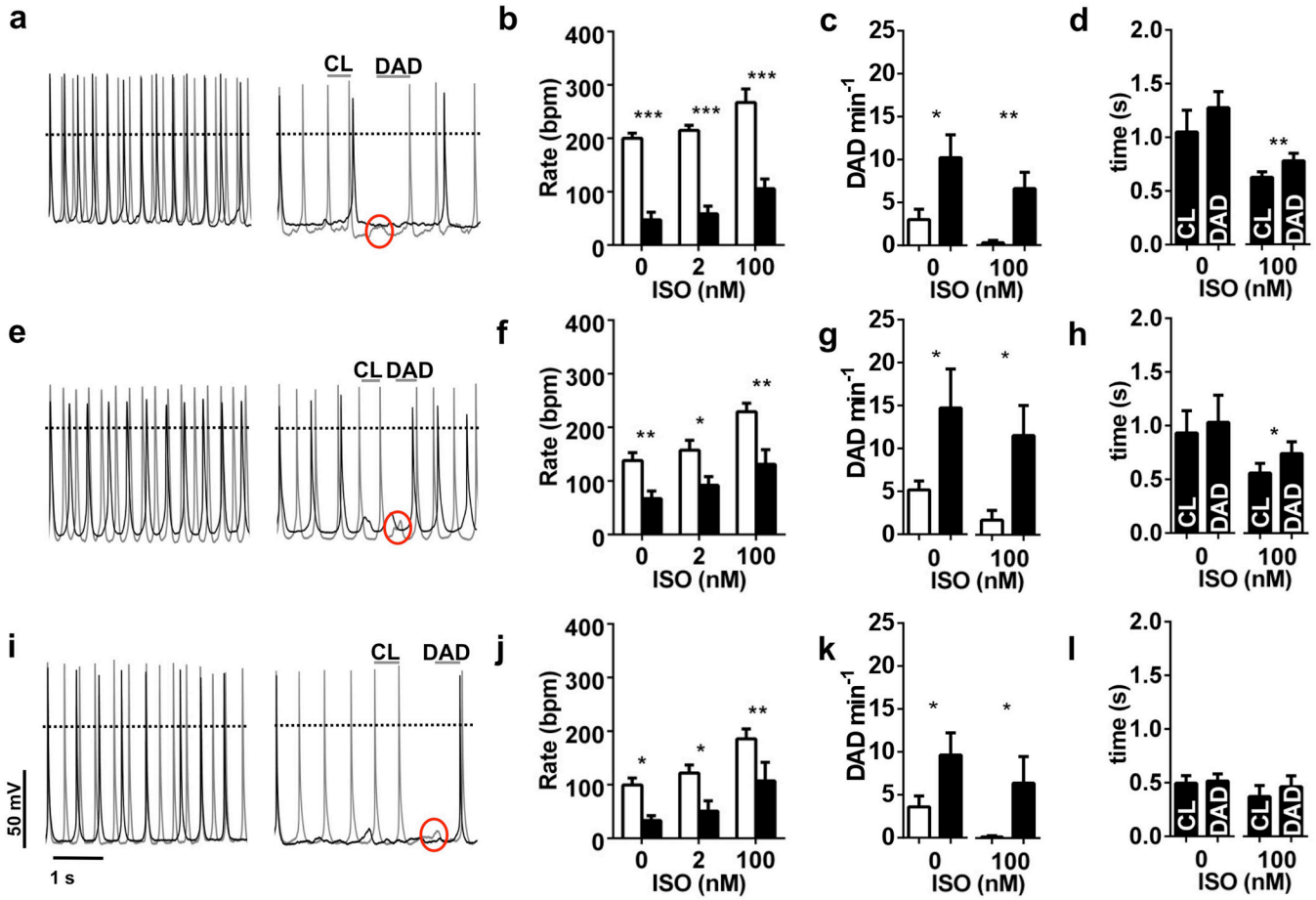

Figure 4. Pacemaker activity and DADs in control and mutant myocytes

(**a**) Action potential recordings of control (**left**) or mutant (**right**) SAN myocytes in Tyrode's solution (black line) and ISO (100 nM, gray line). (**b**) Averaged spontaneous beating rates of SAN myocytes in Tyrode's solution (0; n=11 control, n=11 mutant), ISO 2 nM (n=10 control, n=11 mutant), or 100 nM (n=7 control, n=10 mutant) expressed in beats min^{-1} (bpm). (**c**) Frequency of DADs (defined as a variation of at least 5 mV of the membrane potential) in control and mutant SAN myocytes in Tyrode's solution (n=10 control, n=14 mutant) or ISO 100 nM (n=10 control, n=12 mutant). (**d**) Averaged time interval between a DAD and the following action potential (DAD) in comparison to the cycle length (CL) of the two consecutive action potentials preceding the DAD in n=8 mutant SAN myocytes. (**e**) Action potentials of control (**left**) or mutant (**right**) AVN myocytes in Tyrode's solution (black line) and after ISO (100 nM) perfusion (gray line). (**f**) Spontaneous rates of AVN myocytes in Tyrode's and ISO (0: n=12 control, n=9 mutant cells; 2: n=9 control, n=7 mutant; 100; n=6 control, n=7 mutant). (**g**) Frequency of DADs in control and mutant AVN myocytes in Tyrode's and ISO (0; n=11 control, n=11 mutant; 100; n=11 control, n=13 mutant). (**h**) Same data as in (**d**) for AVN mutant myocytes (0, n=9) and in ISO (100, n=6). (**i**) Spontaneous action potentials recorded from PF myocytes from control (**left**) or mutant (**right**) mice in Tyrode's solution (black line) and after perfusion of ISO (100 nM, gray line). (**j**) Spontaneous beating rates of PF myocytes (0: n=10 control, n=7 mutant; 2: n=9

control, n=6 mutant; 100: n=7 control, n=5 mutant). (**k**) Frequency of DADs in control and mutant PF myocytes (0: n=10 control and n=8 mutant;100: n=5 control, n=7 mutant). (**l**) Same data as in (**d** and **h**) for PF mutant myocytes in Tyrode's solution (n=6) and ISO (n=3) in mutant PF myocytes. Statistics: 2-way ANOVA followed by Sidak multiple comparisons test and unpaired or paired *t*-test. *p<0.05, **p<0.01, ***p<0.001, ****p<0.0001. Error bars indicate S.E.M. Dotted line indicates the 0 mV. Open bars represent data from control, filled bars from mutant mice.

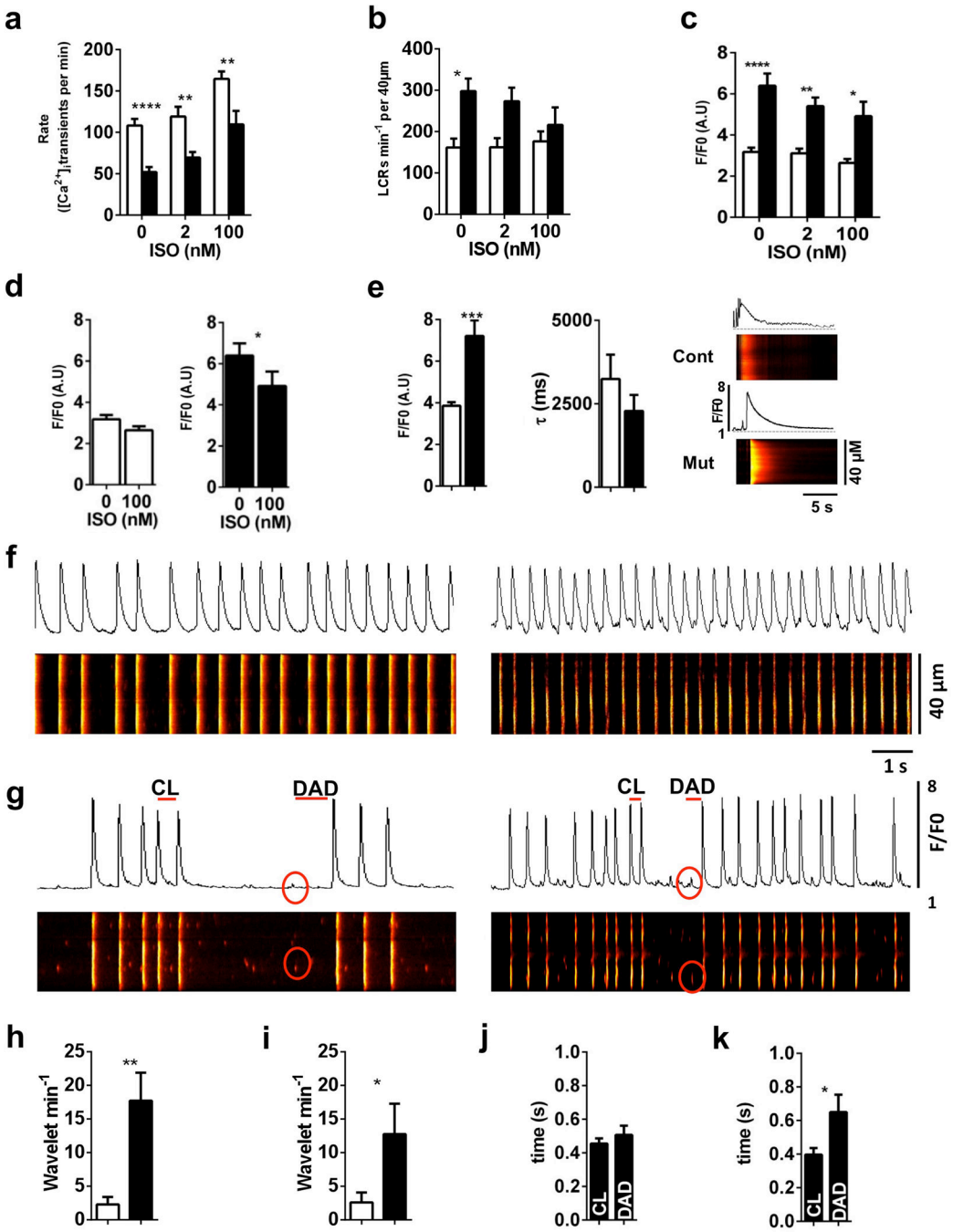

Figure 5. $[Ca^{2+}]_i$ handling in I_f –deficient SAN myocytes

(**a**) Averaged frequency of spontaneous $[Ca^{2+}]_i$ transients of SAN myocytes in Tyrode's solution (n=20 control, n=29 mutant cells), ISO 2 nM (n=16 control, n=29 mutant cells), and in ISO 100 nM (n=14 control, n=12 mutant cells). (**b**) Frequency of LCRs in Tyrode-perfused SAN myocytes (n=19 control, n=24 mutant cells), in ISO 2 nM (n=18 control and n=26 mutant cells), and ISO 100 nM (n=14 control, n=13 mutant cells). (**c**) Averaged amplitude of spontaneous $[Ca^{2+}]_i$ transients of SAN myocytes in Tyrode's solution (n=19 control, n=19 mutant cells), in ISO 2 nM (n=18, n=28 mutant cells), and ISO 100 nM (n=14

control, n=13 mutant cells). Perfusion with ISO reduced transient amplitude in mutant but not in control SAN cells (**d**). Statistics: 2-way ANOVA, followed by Sidak multiple comparisons test. (**e**) Histograms of caffeine-evoked (10 mM) Ca^{2+} release (n=12 control, n=14 mutant cells, **e-left**) and decay (n=9 control, n=11 mutant cells, **e-middle**) in SAN myocytes. **e-right**. Examples of line scan in control (**top**) and mutant (**bottom**) cell during caffeine application. Statistics: unpaired t-test, (**f**) and (**g**) confocal images of spontaneously active control (**f**) and mutant (**g**) SAN myocytes loaded with Fluo-4 perfused with Tyrode's solution (left) or 100 nM ISO (right). Red circle indicates $[Ca^{2+}]_i$ wave, (**h**) and (**i**) averaged frequency of $[Ca^{2+}]_i$ waves (defined as a $[Ca^{2+}]_i$ release larger than 4 μm and/or with an intrinsic light intensity of more than 10% of the intensity measured during the following spontaneous $[Ca^{2+}]_i$ transient) recorded in control and mutant SAN myocytes under Tyrode's solution (n=12 control, n=11 mutant cells, **h**) and ISO 100 nM perfusion (n=12 control, n=11 mutant cells **i**), (**j**) and (**k**) histograms comparing the averaged interval of the cycle length (CL) between two consecutive spontaneous $[Ca^{2+}]_i$ transients preceding the wave and those between the wave and the following spontaneous $[Ca^{2+}]_i$ transient (DAD) in Tyrode's solution (n=11, **j**) and in ISO 100 nM (n=6, **k**) in mutant SAN myocytes. Statistics: t-test. *p<0.05, **p<0.01, ***p<0.001, ****p<0.0001. Error bars indicate S.E.M.

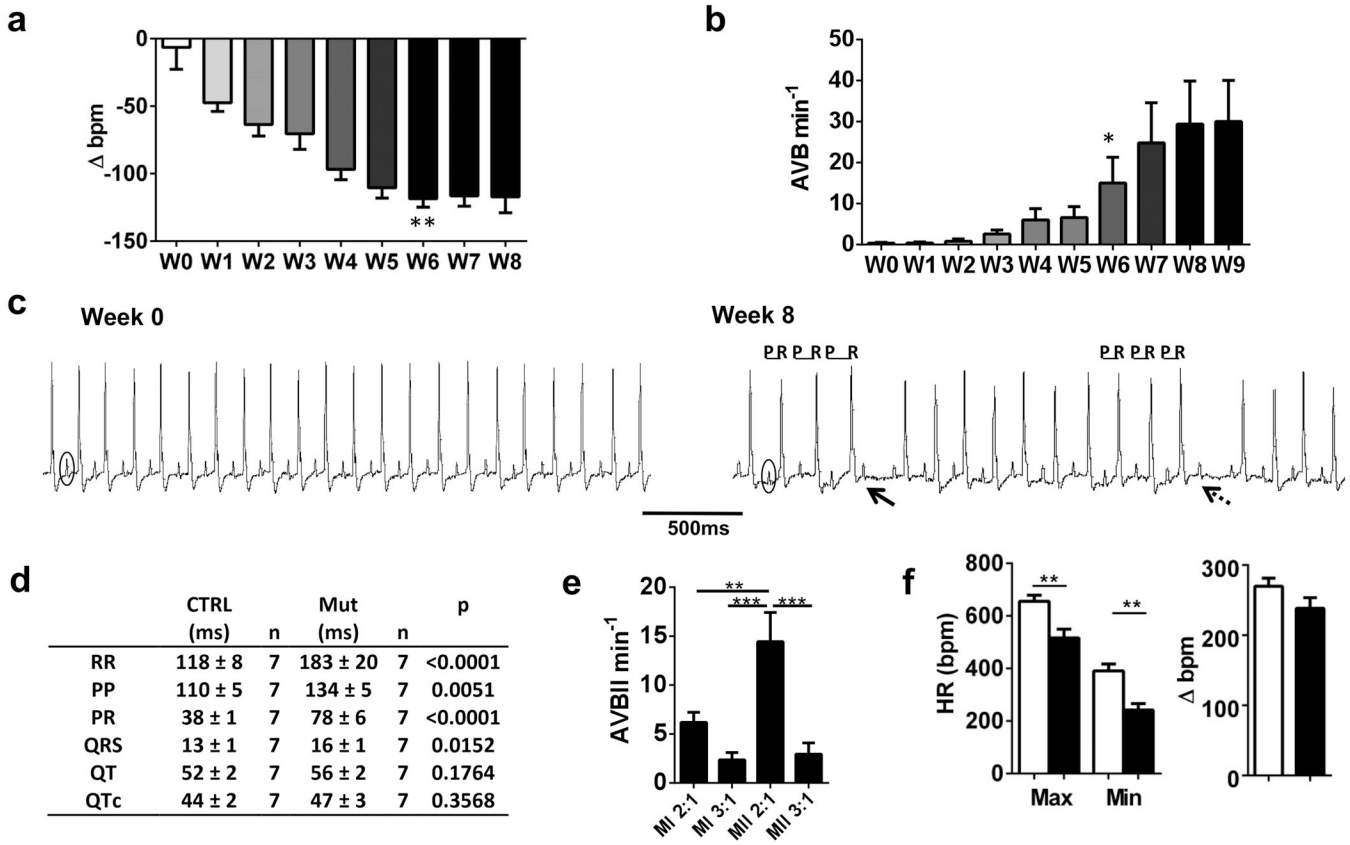

	CTRL (ms)	n	Mut (ms)	n	p
RR	118 ± 8	7	183 ± 20	7	<0.0001
PP	110 ± 5	7	134 ± 5	7	0.0051
PR	38 ± 1	7	78 ± 6	7	<0.0001
QRS	13 ± 1	7	16 ± 1	7	0.0152
QT	52 ± 2	7	56 ± 2	7	0.1764
QTc	44 ± 2	7	47 ± 3	7	0.3568

Figure 6. Time course of heart rate slowing in mutant mice following DOX withdrawal

(**a**) Time course of the heart rate (HR, in bpm) slowing in mutant mice expressed as the difference in heart rate between n=3 control and n=5 mutant mice. DOX was removed from the diet at week 0 (W0). The maximum heart rate difference was observed at week 6 (from 525 ± 16 bpm at week 0 to 429 ± 6 bpm at week 6; *t* test, p<0.001). (**b**) Relationship between the average increase in the number of atrioventricular blocks (AVB) and the time elapsed after DOX withdrawal in n=5 mutant mice (0.2 ± 0.2 AVB/60s at week 0 vs 15 ± 6 AVB/60s at week 6; *t* test, p<0.05). (**c**) Representative examples of ECG traces recorded from mutant mice before (left) and after (right) withdrawal of doxycycline. (**d**) Mean values of ECG intervals recorded from control and mutant mice. Statistics: *t*-test. (**e**) Averaged number of Mobitz type I and type II 2:1 (two P waves for one QRS complex) and 3:1 (three P waves for one QRS complex) AVBs during 30 s of ECG recording (n=9 mutant mice). (**f-left**) Averaged maximum and minimum heart rates in control (open bars) and mutant (filled bars) mice. Statistics: 2-way ANOVA followed by Sidak multiple comparisons test. (**f-right**) Range of heart rate regulation calculated as differences between maximum and minimum heart rates during continuous 24-h ECG recordings of n=7 control and n=9 mutant mice (*t* test, p>0.05). *p<0.05, **p<0.01, ***p<0.001, ****p<0.0001. Error bars indicate S.E.M.

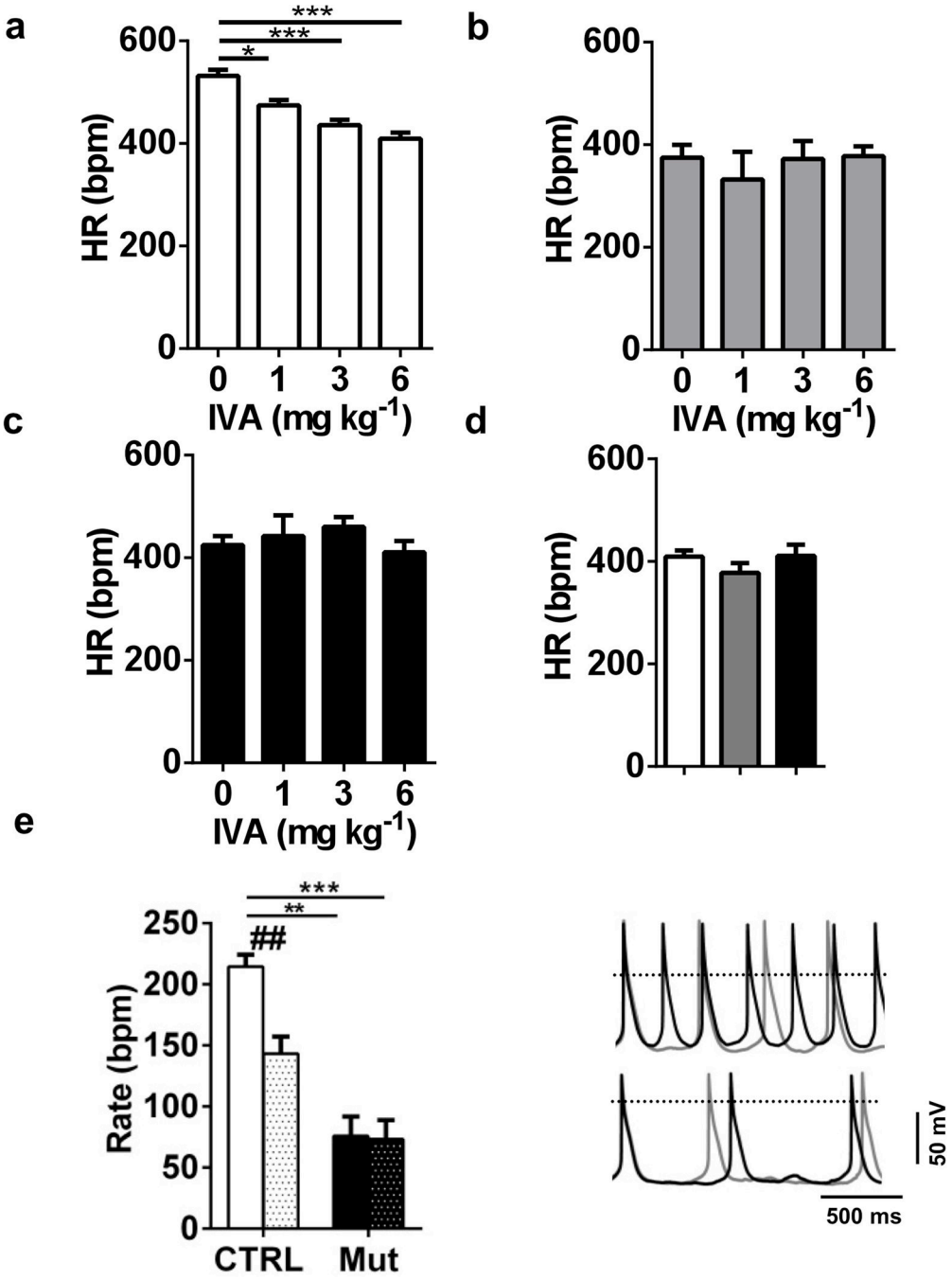

Figure 7. Loss of ivabradine-mediated heart rate reduction in mutant mice

Dose-response relationship of heart rate (RR) to intraperitoneal administration of ivabradine (IVA) in n=13 control (**a**) and n=7 mutant (**b**) mice (ANOVA followed by Tukey's multiple comparisons test). (**c**). Averaged SAN rate (PP interval) in mutant mice after IVA administration. (**d**). Comparison between the SAN rate of control (white bar) and mutant (black bar) mice as compared to the ventricular rate of mutant mice (gray bar) after injection of the highest dose of IVA (6 mg/kg, ANOVA followed by Tukey's multiple comparisons test). (**e-left**) Averaged spontaneous beating rates of SAN myocytes, isolated from n=9

control (white bars) and n=8 mutant mice (black bars), in Tyrode's solution (empty bars) and after perfusion with ivabradine (1 μM, dotted bars). Statistics: 2-way ANOVA followed by Sidak multiple comparisons test. *p<0.05, **p<0.01, ***p<0.001, ****p<0.0001. Error bars define the S.E.M. (**e-right**) Sample action potentials recorded from control (top) and mutant (bottom) SAN myocytes before (black line) and after (gray line) application of 1 μM ivabradine.

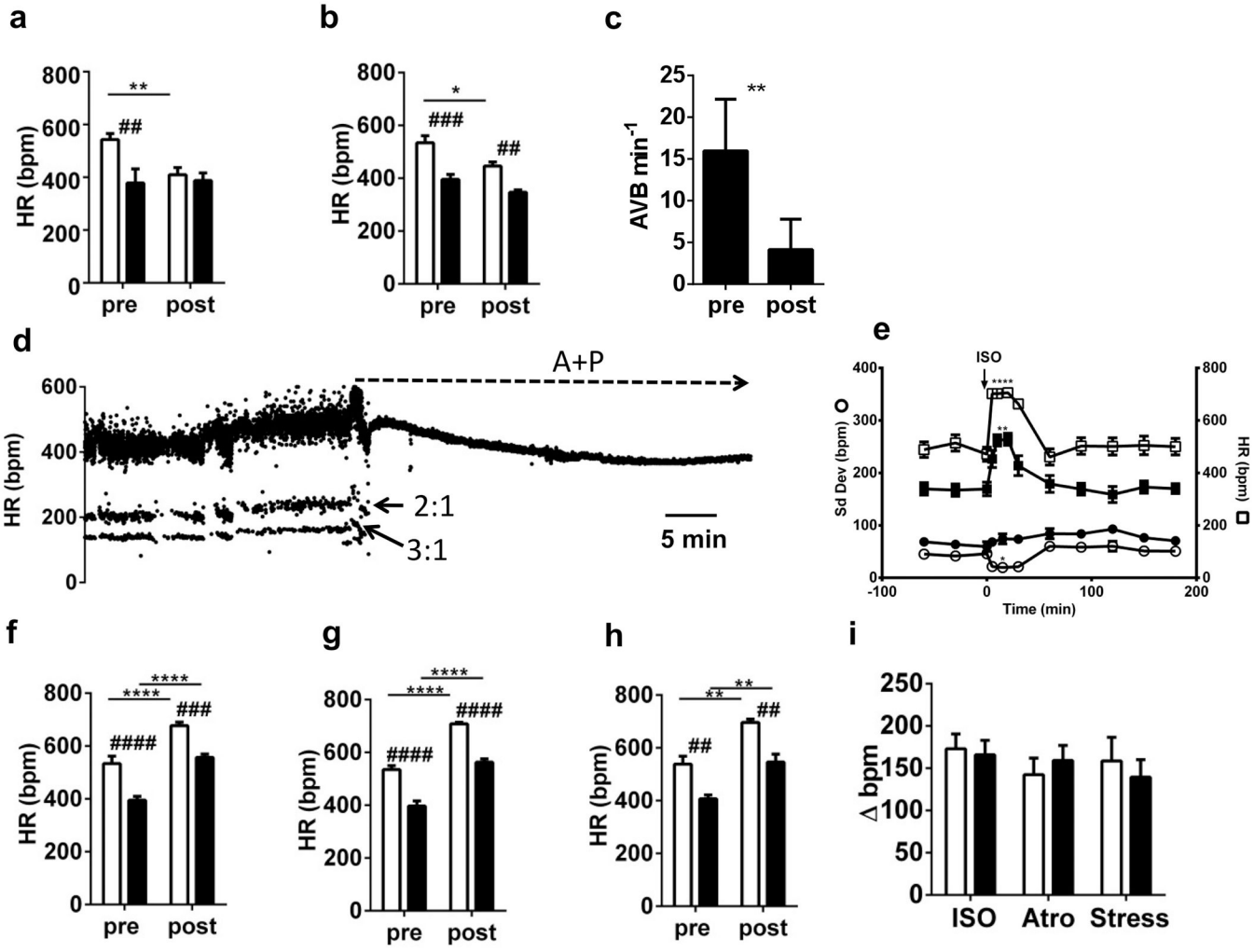

Figure 8. Autonomic regulation of heart rate and impulse conduction in mutant mice

Averaged heart rate recorded from n=11 control (open bars) and n=11 mutant (filled bars) mice before (pre) and after (post) intraperitoneal injection of propranolol (**a**), or atropine and propranolol (**b**). Statistics in (**a**) and (**b**): 2-way ANOVA followed by Sidak multiple comparisons test. (**c**). Number of atrioventricular blocks (AVB) measured in a 30-s window every 5 minutes for a 30-min total recording period before (pre) and after (post) injection. AVB counting started 30 minutes after injection to allow the effect to stabilize. Statistics: *t*-test. (**d**). Sample dot plot of beat-to-beat variability (bpm) of heart rate of mutant mice before and after (dotted line) injection of atropine and propranolol. Note slow ventricular beats in the presence of AVB before injection. Arrows indicate AVBs (two P waves for one QRS complex, 2:1; three P waves for one QRS complex, 3:1). (**e**). Time course of heart rate and the standard deviation of heart rate before and after injection of ISO. (**f–h**). Heart rate in control and mutant mice before and after injection of atropine (**f**) or isoproterenol (**g**) in n=8 control and n=12 mutant mice. (**h**) Heart rate before and after 5-min swimming test, in n=5 control (open bars) and n=7 mutant (filled bars) mice. (**i**) Delta of heart rate following different β-adrenergic stimulation. Values represent the mean difference between pre- and post-adrenergic pathway activation (pharmacological or physiological). Statistics: 2-way

ANOVA followed by Sidak multiple comparisons test. *p<0.05, **p<0.01, ***p<0.001, ****p<0.0001. Error bars indicate S.E.M.

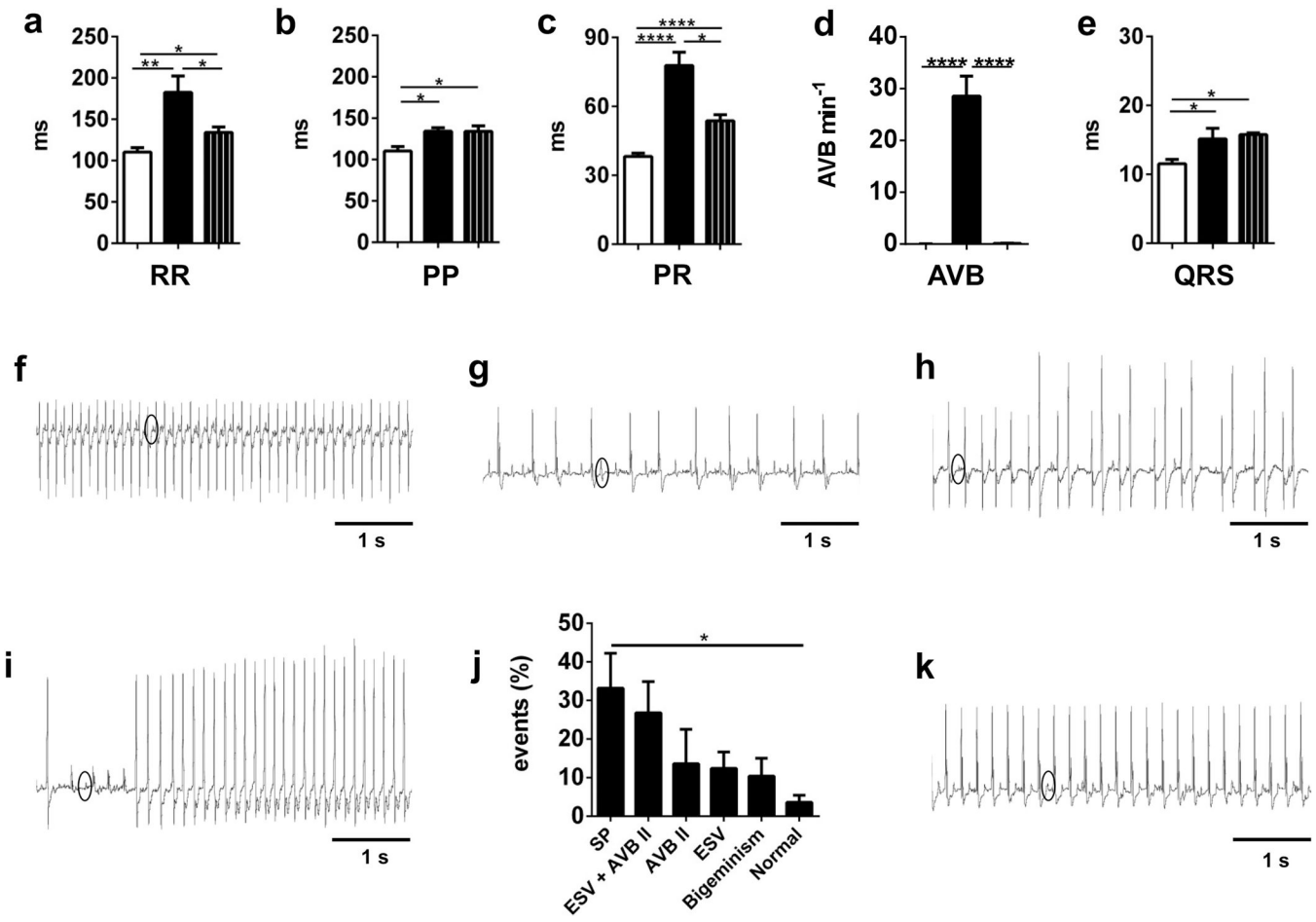

Figure 9. Improvement of heart rate in mutant mice by *GIRK4* gene knockout

Averaged RR (**a**), PP (**b**), PR (**c**), number of atrioventricular blocks (AVB) (**d**) and QRS (**e**) in n=7 control (white bar), n=7 mutant (black bar), and n=8 Mut/*GIRK4*$^{-/-}$ (black bar with white stripes) mice. Statistics (**a–e**): ANOVA followed by Tukey's multiple comparisons test. *p<0.05, **p<0.01, ***p<0.001, ****p<0.0001. Error bars define the S.E.M. **f**. Representative example of ECG recordings from control mice. (**g–i**). Different examples of ECG recordings showing heart rate dysfunction recorded from mutant mice. (**g**) Second-degree AVB; (**h**) ventricular extrasystoles; (**i**) ventricular tachycardia. (**j**) Relative percentages of SAN or AVN dysfunctions preceding a period of ventricular tachycardia in n=5 mutant mice (SP: sinus pauses, ESV: ventricular extrasystoles). (**k**) ECG recorded from Mut/*GIRK4*$^{-/-}$, mice. Small circles indicate P waves.

Table 1

Summary table of the fraction of control (CTRL), mutant (Mut) or Mut/*GIRK4*$^{-/-}$ mice with heart rhythm disturbances. AVB: atrioventricular block; ESV: ventricular extrasystole; VT: ventricular tachycardia. Statistics: Chi^2 test.

	CTRL	Mut	Mut/*GIRK4*$^{-/-}$	p
Sinus pauses	0/12	5/13	0/8	0.0408
Bradycardia	0/12	13/13	8/8	0.0009
AVB I degree	0/12	13/13	0/8	0.0009
AVB II degree	0/12	13/13	0/8	0.0009
AVB III degree	0/12	13/13	0/8	0.1293
ESV	0/12	4/13	0/8	0.0715
VT	0/12	5/13	0/8	0.0408